

AD-A189 422

TWO-PHASE FLOWS IN THE WAKE OF IN-CYLINDER PROJECTILES
(U) IMPERIAL COLL OF SCIENCE AND TECHNOLOGY LONDON
(ENGLAND) J H WHITELAW DEC 87 R/D-4352-R-AM

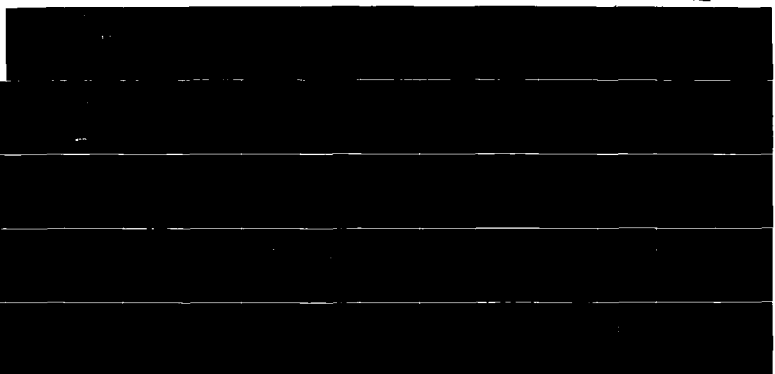
1/1

UNCLASSIFIED

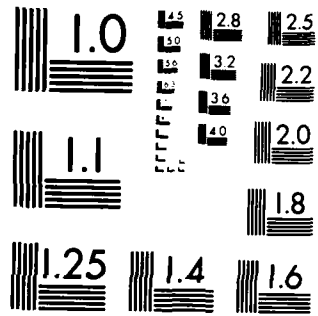
DAJA45-84-C-0032

F/G 19/10

ML



END
-1-
JAN 88



MICROCOPY RESOLUTION TEST CHART
NATIONAL BUREAU OF STANDARDS-1963-A

DTIC FILE COPY

4

AD-A189 422

TWO-PHASE FLOWS IN THE WAKE OF IN-CYLINDER PROJECTILES

Final Technical Report

by

J H Whitelaw

December 1987

DTIC
ELECTE
DEC 30 1987
S D

United States Army

EUROPEAN RESEARCH OFFICE OF THE US ARMY

LONDON, ENGLAND.

CONTRACT DAJA 45-84-C-0032

IMPERIAL COLLEGE OF SCIENCE AND TECHNOLOGY

LONDON, ENGLAND.

Approved for Public Release; distribution unlimited

87

Unclassified
SECURITY CLASSIFICATION OF THIS PAGE

REPORT DOCUMENTATION PAGE				Form Approved OMB No 0704-0188 Exp Date Jun 30 1986	
1a REPORT SECURITY CLASSIFICATION Unclassified		1b RESTRICTIVE MARKINGS A189422			
2a SECURITY CLASSIFICATION AUTHORITY		3 DISTRIBUTION/AVAILABILITY OF REPORT Approved for public release; distribution unlimited			
2b DECLASSIFICATION/DOWNGRADING SCHEDULE					
4 PERFORMING ORGANIZATION REPORT NUMBER(S)		5 MONITORING ORGANIZATION REPORT NUMBER(S) R&D 4352-R-AN			
6a NAME OF PERFORMING ORGANIZATION Imperial College of Science and Technology		6b OFFICE SYMBOL (if applicable)	7a NAME OF MONITORING ORGANIZATION USARDSG(UK)		
6c ADDRESS (City, State, and ZIP Code) Exhibition Road London SW7 2BX		7b ADDRESS (City, State, and ZIP Code) Box 65 FPO New York 09510-1500			
8a NAME OF FUNDING/SPONSORING ORGANIZATION Ballistic Research Laboratory		8b OFFICE SYMBOL (if applicable) SLCBR-IB	9 PROCUREMENT INSTRUMENT IDENTIFICATION NUMBER DAJA45-84-C-0032		
8c ADDRESS (City, State, and ZIP Code) U.S. Army Laboratory Command Aberdeen Proving Ground, MD 21005-5066		10. SOURCE OF FUNDING NUMBERS	PROGRAM ELEMENT NO. 61102A	PROJECT NO 1L161102BH	TASK NO 7 06
			WORK UNIT ACCESSION NO		
11 TITLE (Include Security Classification) (U) Two-phase Flows in the Wake of In-cylinder Projectiles					
12 PERSONAL AUTHOR(S) J. H. Whitelaw					
13a TYPE OF REPORT Final		13b TIME COVERED FROM Jul 84 TO Oct 87		14 DATE OF REPORT (Year, Month, Day) 1987, September Dec.	15 PAGE COUNT 76
16 SUPPLEMENTARY NOTATION					
17 COSATI CODES			18 SUBJECT TERMS (Continue on reverse if necessary and identify by block number)		
FIELD	GROUP	SUB-GROUP			
20	04				
20	06				
19. ABSTRACT (Continue on reverse if necessary and identify by block number) Measurements of local velocity of the flow and of 500µm solid particles have been obtained in gun simulators and have provided guidance for the design and construction of a new rig which allows projectile velocities up to 500m/s. The relationship between breech pressure and projectile velocity is shown to be described by one-dimensional, unsteady forms of the conservation equations; the wall boundary layer is turbulent and the effect of chamber geometry is small; and the lag of the particles behind the fluid in regions close to the projectile is of order 20%. The results are suitable for comparison with those obtained from calculation methods.					
20 DISTRIBUTION/AVAILABILITY OF ABSTRACT <input checked="" type="checkbox"/> UNCLASSIFIED/UNLIMITED <input checked="" type="checkbox"/> SAME AS RPT <input checked="" type="checkbox"/> DTIC USERS			21 ABSTRACT SECURITY CLASSIFICATION Unclassified		
22a NAME OF RESPONSIBLE INDIVIDUAL Dr. Fritz H. Oertel, Jr.			22b TELEPHONE (Include Area Code) 01-409 4423	22c OFFICE SYMBOL AMXSN-UK-RA	

DD FORM 1473, 84 MAR

83 APR edition may be used until exhausted
All other editions are obsolete

SECURITY CLASSIFICATION OF THIS PAGE
Unclassified

purposes of improved understanding of the flow and of calculation methods. These aspects of the work are not considered in this report and it should be emphasised that they were essential to the determination of the results and provide the basis for the intended future work with the high-speed rig.

The results obtained in the three gun-simulation rigs are discussed briefly in the following section and further details are available in the references cited. The report ends with a summary of the more important conclusions.

Results obtained in gun-simulation experiments

Preliminary measurements in the first rig, see figure 1, indicated the main features of in-cylinder flows for initial pressures up to 9 bars. The near-wall measurements revealed thin boundary layers and the maximum velocity fluctuations in the bulk flow grew from zero to around 6% as shown in figure 2. They were the first available measurements for in-cylinder flows caused by a moving projectile and were used at BRL to support the development of the Δ code. They also showed that improvements could be made to the rig and the instrumentation so as to permit more accurate results at higher pressures. The instrumentation used with the first rig included a pressure transducer, laser velocimeter and optical encoder, but the transducer signal was not digitised or multiplexed, the velocimeter was not arranged specifically for the gun simulator and the encoder operated from a mechanical rack and pinion.

The second rig was designed and constructed to allow more detailed measurements in the near-wall region and operation without the drag force associated with the rack-and-gear mechanism. Improvements were also made to involve higher pressures, to allow the introduction of particles in a quantitatively known way and to allow the release of the projectile in a manner which could also be used in the third rig, proposed for use with much higher pressures. The method of measuring the projectile velocity was changed to make use of an optical technique and the laser-velocimeter was rearranged with higher power laser and faster signal processing; these two electro-optic devices were designed so that they could also be used with the third rig. The second rig is shown in figure 3.

The measurements of reference 3 and 4 were obtained in the second rig and, as can be seen from figure 4 for example, the near-wall velocity traces exhibit increasing velocity fluctuations as the wall is approached. The ensemble-averaged boundary-layer profiles follow clearly a power law with index varying from 6.6 to 9.9 as the projectile progresses down the barrel. These results, and the calculated shape factors which varied from 1.2 to 1.3, confirm that the boundary-layer is turbulent with characteristics similar to those of a steady turbulent boundary layer. The results of reference 3 provide a well-defined picture of the flow in the simulated gun with an initial condition corresponding to quiescent flow. They were extended, in reference 4, to involve single- and two-phase flows, which involve flow into the breech through an array of jets, and confirm that the geometry of the initial chamber does not affect the downstream flow properties.

The two-phase flow experiments involved 500 μm diameter particles with initial volume concentrations up to 1.3%. A sample of the results is shown on figure 5 and allows comparison with those obtained without the particles. The results were obtained at the first, second and third windows corresponding to axial locations of 4.96, 7.90 and 10.84d. It can be seen that the solid particles lag behind the fluid by times which increase with axial distance, i.e., as the projectile is approached. The difference between fluid and particle velocity increases in the bulk flow from about 1 m/s and $x/d = 4.96$ and $t = 20.5$ ms to 8 m/s (21%) at $x/d = 10.84$ at $t = 27.5$ ms. The lag is due to inertial effects associated with solid particles in a strongly accelerated flow field and can be expected to be much greater at the accelerations of the third rig and of guns.

The work of reference 5 was carried out to determine the effect of a three-fold increase in particle concentration, to re-examine the near-wall region and to test procedures which are to be used in the third rig. The measurements in the near-wall region have confirmed the turbulent nature of the wall boundary layer and the increase in particle concentration has shown a tendency for the particles on the centre line to decrease in velocity less rapidly than with the lower concentrations examined previously. The instrumentation and experimental techniques proved satisfactory and led to the arrangement of the third rig, as shown on figure 6. Preliminary tests with this rig have confirmed that the

projectile velocity corresponds to values determined with isentropic-flow assumptions, as shown on figure 7, and that values of over 400 m/s can readily be attained.

The preparations for future work include the provision of a high-speed counter, an argon-ion laser and a Bragg cell optical unit. The software has been prepared and provision made for the necessary interface between the centre and IBM AT computer. In addition, the related efforts of reference 6 has quantified the influence of particles in liquid with volume concentrations up to around 0.15 and references 7 to 10 provided instrumentation for the simultaneous measurement of the discrete and carrier phase with known accuracy. Work is in progress to determine the accuracy with which the barrel temperature can be measured as the projectile passes downstream.

Conclusions

The following paragraphs provide a summary of the more important conclusions:

1. The first and second gun simulators, and related instrumentation, have provided information of the velocity characteristics of projectile and gas as a function of projectile position and initial pressure. The experiments have provided guidance for the design and construction of a third rig, and related instrumentation, which will allow projectile velocities up to 500 m/s.
2. The relationship between breech pressure and projectile velocity is shown to be described by one-dimensional, unsteady forms of the continuity and momentum equations. The measured record of breech pressure leads to calculated values of projectile velocity within 0.5% of the measured values and confirms that friction between projectile and tube wall is negligible.
3. The velocity results, for single- and two-phase flows, are provided in sufficient detail to aid the development and appraisal of calculation methods, based on the numerical solution of conservation equations in differential form. They quantify the variation of gas and particle velocity as a function of position and time and quantify its decay

after the passage of the projectile. The wall boundary layer is shown to be turbulent and the lag between 500 μm solid particles and the gas phase quantified for two values of concentration.

4. The effect of initial chamber geometry is shown to be small at the comparatively low velocities of the two simulators.
5. The experimental and measurement techniques have been shown to be appropriate and will be used in a subsequent investigation in a third rig with much higher pressures and velocities. This rig has been constructed and tested. Preliminary measurements confirm conclusion 2 and show that it will be possible to extend the research to projectile velocities in excess of 500 m/s, which overlaps with the lower limit of the related experimental program at the Ernst Mach Institute. This third rig has been designed to permit measurements with pellets to solid propellant to assist the acceleration of the projectile and related two-phase flow instrumentation has been developed and tested.

References

1. A F Bicen and J H Whitelaw (1984). Velocity characteristics of the wakes of an in-cylinder projectile. Presented at International Congress on Instrumentation in Aerospace Simulation Facilities, ISL, St Louis, France.
2. A F Bicen, Y Kliafas and J H Whitelaw (1985). In-Bore velocity measurements in the wake of subsonic projectile. AIAA Paper, 85-1676. See also AIAA J 24, 1035, 1986.
3. A F Bicen, L Khezzar and J H Whitelaw (1987) Subsonic single-phase flow in a gun simulator. Imperial College, Mechanical Engineering Department Report FS/86/03. Submitted to AIAA Journal.
4. A F Bicen, L Khezzar and J H Whitelaw (1986). Subsonic single- and two-phase flow characteristics of a gun simulator. Imperial College, Mechanical Engineering Department Report FS/86/43.

5. M Schmidt (1987). Subsonic single- and two-phase flow characteristics with increased particle loading of a gun simulator. Imperial College, Mechanical Engineering Department Report FS/87/29.
6. J M Nouri, J H Whitelaw and M Yianneskis (1987). Particle motion and turbulence in dense two-dimensional flows. *J Multiphase Flow*, accepted for publication.
7. Y Kliafas, A M KP Taylor and J H Whitelaw (1986). The influence of depth of field on particle sizing by LDA. *Experiments in Fluids* 5, 159.
8. Y Kliafas, A M KP Taylor and J H Whitelaw (1986). Errors due to turbidity in particle sizing using laser-Doppler velocimetry. AIAA/ASME 4th Joint Fluid Mechanics Conference, Atlanta.
9. Y Hardalupas (1986). Phase-Doppler anemometry for simultaneous particle size and velocimetry measurements. Imperial College, Mechanical Engineering Department Report FS/86/14.
10. Y Hardalupas, A M K P Taylor and J H Whitelaw (1986). Depth of field considerations in particle sizing using the phase-Doppler technique. Laser Anemometry in Fluid Mechanics III, LADOAN, Portugal.

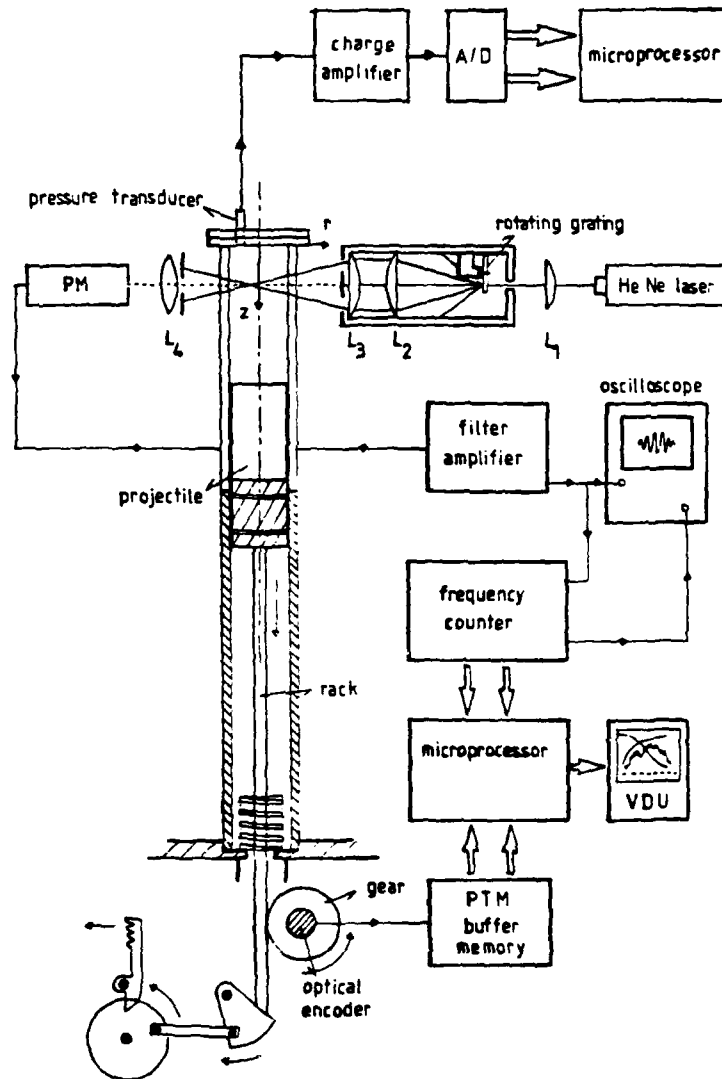


Figure 1 Arrangement of first projectile rig

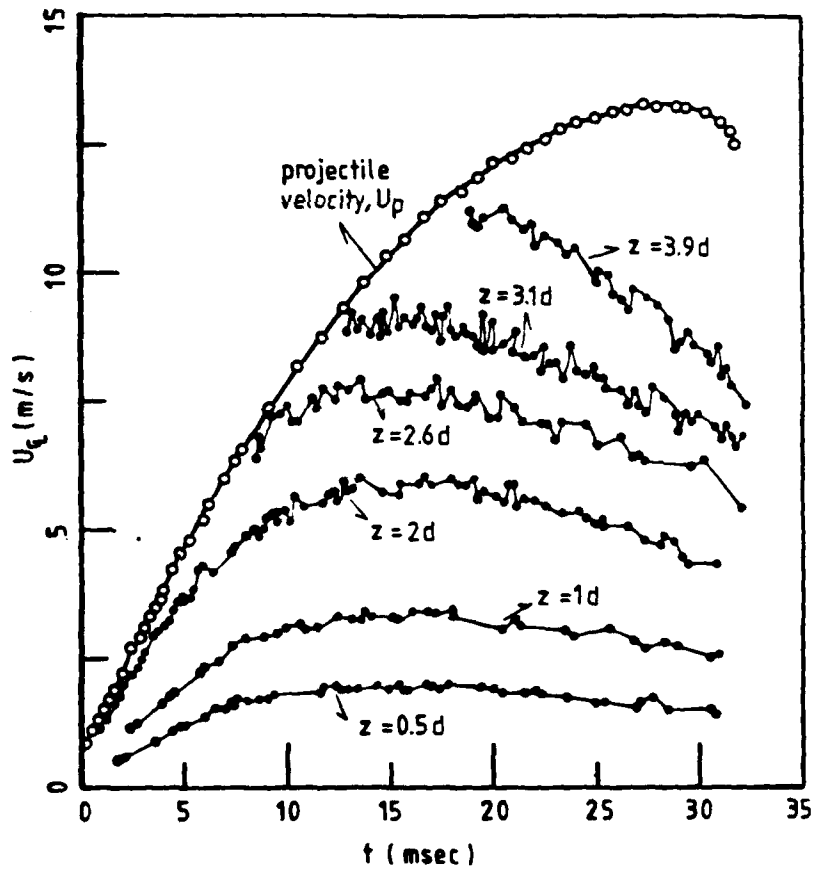


Figure 2 Centre-line velocity traces

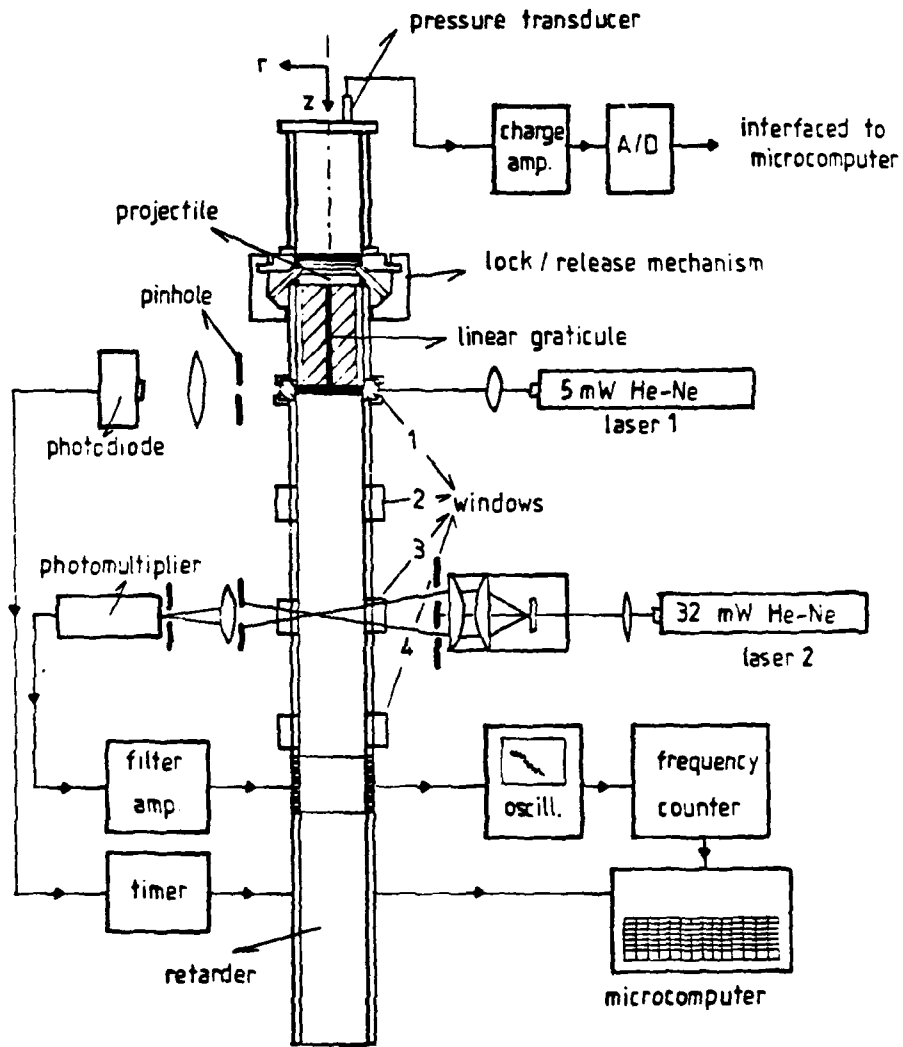


Figure 3 Arrangement of second projectile rig

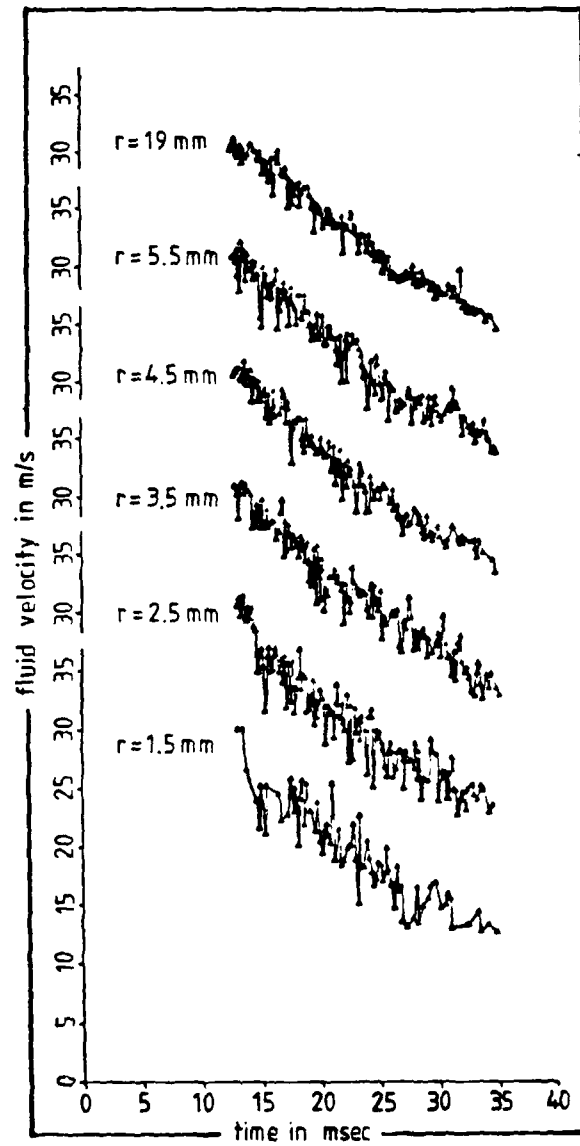


Figure 4 Velocity variation with time and distance from the wall

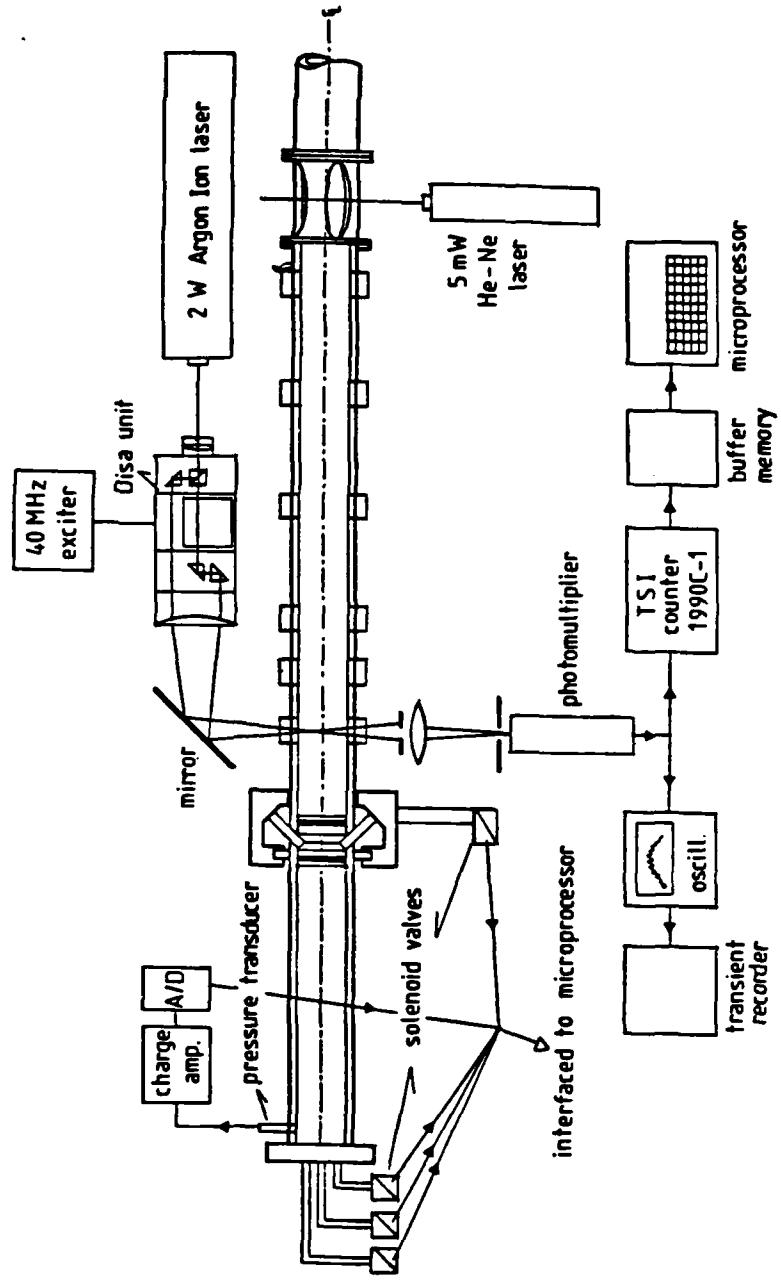


Figure 6 Arrangement of third projectile rig

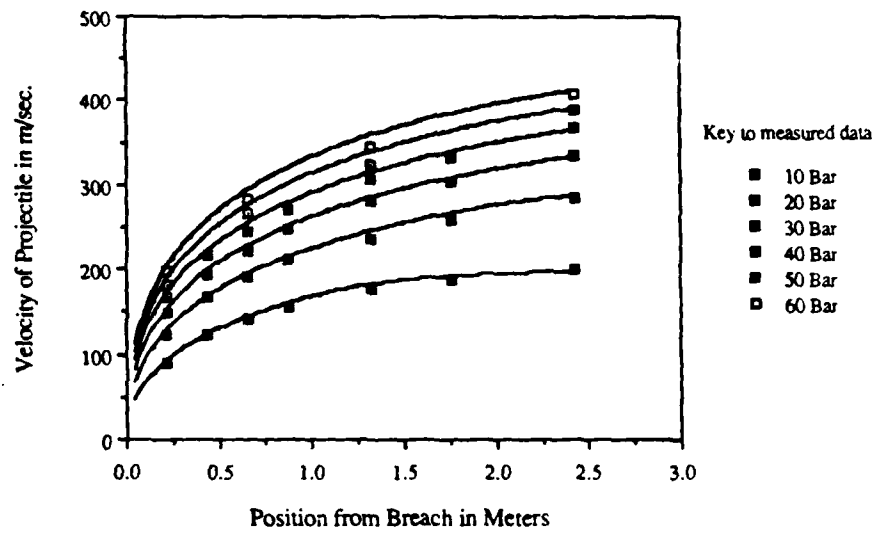


Figure 7 Isentropic-flow predictions and measurements of projectile velocity

**In-Bore Velocity Measurements in the Wake
of a Subsonic Projectile**

A. F. Bicen, Y. Kliafas, J. H. Whitelaw

Appendix

The integral forms of the momentum and energy solutions are obtained below for the case where freestream vorticity and total enthalpy gradients are included in the boundary-layer solution. From Eqs. (1) and (2), and (8),

$$\tau_0 = \int_0^{\delta} \{ u'' [\rho u]'' - \rho u \} + \{ \rho u (u'' - u) \} + u'' \{ \rho v \}'' - \rho v + \{ \rho v (u'' - u) \} \} dy \quad (A1)$$

Equation (A1) together with Eqs. (1), (10), and (7a) then gives

$$\tau_0 = (u_1)_{y=0} \int_0^{\delta} \{ (\rho u)'' - \rho u \} dy - \frac{d}{dx} \omega_0 \int_0^{\delta} \{ (\rho u)'' - \rho u \} y dy + \frac{d}{dx} \int_0^{\delta} \rho u (u'' - u) dy \quad (A2)$$

Similarly, from Eqs. (1), (4), (7b), and (10),

$$q_0 = \int_0^{\delta} \{ H'' [\rho u]'' - \rho u \} + \{ \rho u (H'' - H) \} + H'' \{ \rho v \}'' - \rho v + \{ \rho v (H'' - H) \} \} dy = (H_1)_{y=0} \int_0^{\delta} \{ (\rho u)'' - \rho u \} dy + \frac{d}{dx} (H_1)_{y=0} \times \int_0^{\delta} \{ (\rho u)'' - \rho u \} y dy + \frac{d}{dx} \int_0^{\delta} \rho u (H'' - H) dy \quad (A3)$$

References

¹Melnik, R. E., "Turbulent Interactions on Airfoils at Transonic Speed—Recent Developments," *Computation of Viscous-Inviscid Interactions*, AGARD CP-291, Oct. 1980, Paper 10
²Johnston, W. and Sokol, P., "Matching Procedure for Viscous-Inviscid Interactive Calculations," *AIAA Journal*, Vol. 17, June 1979, pp. 661-663.
³Murman, E. M. and Bussing, T. R. A., "On the Coupling of Boundary Layer and Euler Equation Solutions," *2nd Symposium on Numerical and Physical Aspects of Aerodynamic Flows*, 1983, edited by T. Cebeci, Springer-Verlag, New York, 1984, pp. 313-326
⁴Van Dyke, M., *Perturbation Methods in Fluid Mechanics*, Academic Press, New York, 1964

In-Bore Velocity Measurements in the Wake of a Subsonic Projectile

A.F. Bicen,* Y. Klifas,† and J.H. Whitlaw‡
 Imperial College of Science and Technology
 London, England

Introduction

VELOCITY and pressure have been measured in the flow behind a projectile traveling in a tube and propelled by compressed gas. The arrangement is intended to simulate that

Received April 10, 1985, presented as Paper 85-1676 at the AIAA 18th Fluid Dynamics, Plasmas and Lasers Conference, Cincinnati, OH, July 16-18, 1985, revision received Aug. 26, 1985. Copyright © American Institute of Aeronautics and Astronautics, Inc., 1985. All rights reserved.

*Research Fellow, Department of Mechanical Engineering
 †Research Assistant, Department of Mechanical Engineering
 Member AIAA.
 ‡Professor, Department of Mechanical Engineering

of interior ballistics, with nonreacting flow and projectile velocities up to 21 m/s. Although the real processes are much more complex and involve a continuous interaction of two phases (solid gas or liquid gas) through a combustion process, the present simplified experiments serve to provide fundamental understanding of the flow behind in-bore projectiles and thereby support the development of phenomenological models, such as those of Refs. 1 and 2, and multidimensional solution methods such as that of Ref. 3.

A projectile was secured in position inside a tube pressurized by compressed gas to a required pressure. After the gas had become quiescent, the projectile was released. The pressure in the tube and the projectile velocity were measured, together with the local velocity of the fluid obtained with a laser velocimeter, as a function of time. The experiment was repeated at different locations until a satisfactory picture of the flow had been assembled. The initial pressure was regarded as a variable so as to determine the extent to which the flow properties varied with projectile velocity, and the experiment was conducted with two initial chambers of different length.

Experimental System

The flow arrangement and related instrumentation are shown in Fig. 1. The measurements were obtained in the cavity formed by a 76.7-mm-diam tube, a blanked end, and a 76.4-mm-diam projectile that had a flat end. The effect of initial chamber length was investigated by using two different lengths of 177.3 and 311 mm, which were achieved by altering the projectile overall length. The upper 300 mm of the tube was made of plexiglass and the remaining part of mild steel with the gap between the projectile and tube wall sealed by two silicon-rubber rings. The projectile was allowed to travel for a distance of approximately 400 mm before being retarded by a series of compression springs.

The initial gas pressure P_0 ranged from 2.91 to 9.1 bars and was achieved with nitrogen taken from a pressurized cylinder.

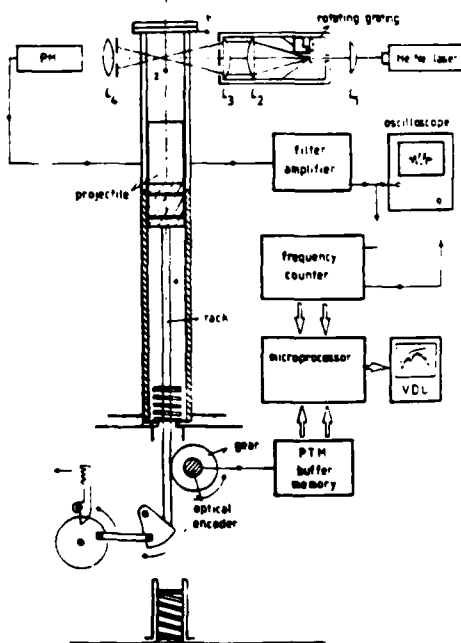


Fig. 1 Schematic diagram of experimental system.

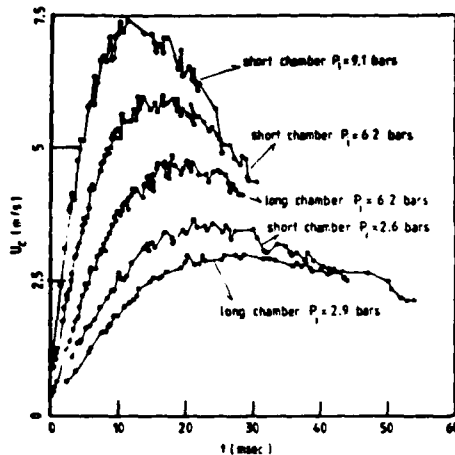


Fig. 2 Centerline velocity traces at $z = 153.4$ mm for two initial chamber lengths and various initial pressures.

The initial pressure and the variation of pressure with time were measured, with a precision of ± 0.002 bar, using a piezoelectric transducer and a charge amplifier whose output was digitized and interfaced to a microprocessor.

Laser Doppler anemometry was used to obtain the fluid velocities with the optical arrangement of Ref. 4. Silicon oil droplets, served as light-scattering particles, were introduced in the initial chamber prior to the charging of the volume with the pressurized gas.

The frequency of the Doppler signal was measured by a purpose-built frequency counter also interfaced to the microprocessor. The time information corresponding to each frequency count was obtained from a Programmable Time-Module initiated to time at a rate of 417 KHz after the first 1-mm travel of the projectile.

The projectile position was determined by an optical encoder coupled to the rack and gear arrangement of Fig. 1, and each encoder pulse corresponded to an axial distance of 0.2 mm. The time between two consecutive pulses was measured by a high-frequency crystal clock oscillating at a rate of 1.0 MHz, and values were stored in a buffer memory.

The data stored were subsequently processed by the microprocessor to determine and display the variation of projectile and local flow velocity and pressure as a function of time. The accuracy of fluid velocity measurement is expected to be of the order of 1% except in the near-wall region where velocity-gradient broadening became important and, with the present optical arrangement, precluded useful results within around 0.5 mm of the wall.

Results and Discussion

The traces of centerline velocity U_c , measured at an axial distance of 153.4 mm from the closed end, are shown in Fig. 2 for both chambers and for a range of initial pressures. The velocities with the larger initial volume are lower, since the measurement location is farther from the projectile. It is also evident that each velocity trace is initially associated with a monotonic increase and that fluctuations gradually appear with decreasing acceleration. The root-mean-square value of these fluctuations is around 3%, with normalized peak-to-peak values of about 6%.

Centerline velocity traces are also shown in Fig. 3 for the short initial chamber and initial pressure of 6.2 bars. The

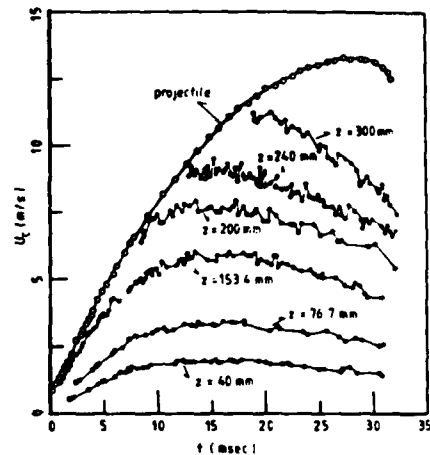
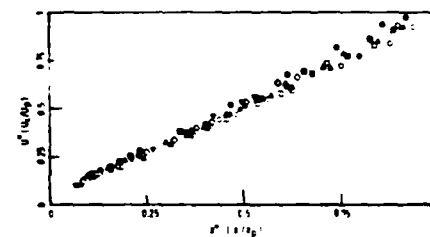


Fig. 3 Centerline velocity traces at various axial locations for short initial chamber and $P_1 = 6.2$ bars.



Plots of nondimensional centerline velocity U^* against nondimensional axial distance z^* for long chamber and $P_1 = 2.91$ bars; $z^* = 5, 10, 20, 30,$ and 40 ms; for long chamber and $P_1 = 6.2$ bars; $z^* = 5, 10,$ and 20 ms; for short chamber and $P_1 = 6.2$ bars; $z^* = 5, 10$ and 20 ms.

results include some of those of Fig. 2, extend to larger values of axial distance, and include positions initially occupied by the projectile. The fluid velocity increases with axial distance and in accord with the accelerating projectile. At positions initially occupied by the projectile, the velocity decays after the projectile has passed, at a rate that increases with the axial distance. The results confirm the tendency of the fluid velocities to fluctuate with an amplitude that appears to increase until a peak-to-peak value of around 6% is achieved.

Figure 4 shows the nondimensional centerline velocity U^* (U_c/U_p) plotted against the nondimensional axial distance z^* (z/z_p) for different initial pressures, chamber lengths, and times in the cycle; U_p and z_p are the corresponding projectile velocity and position, respectively. The figure clearly demonstrates that the fluid velocity distribution between the breech and the projectile base is linear and scales with the projectile velocity at all times in the cycle, for the range of initial pressures and two chamber lengths considered here.

Radial profiles of velocity were obtained from velocity traces such as those of Fig. 5 and were found to be nearly uniform apart from thin regions near the wall boundaries.⁵ The traces of Fig. 5 correspond to locations 0.5, 1, and 2 mm from the wall with the velocity values at $r_w = 0.5$ mm generally of the order of 90-94% of the velocities at $r_w = 2$ mm. The

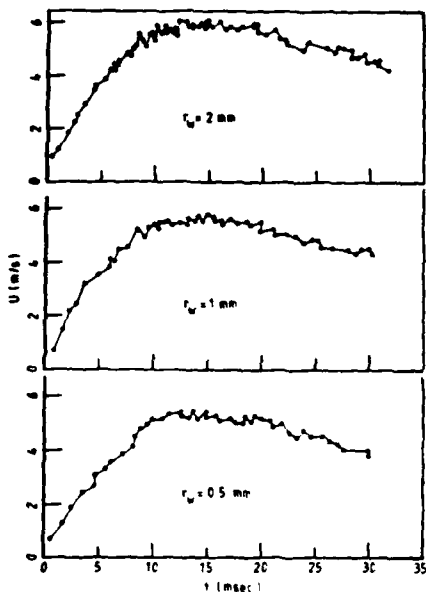


Fig. 3 Fluid velocity traces near wall boundary at $z = 153.4$ mm for short initial chamber and $P_i = 6.2$ bars.

boundary-layer thickness was found to be less than 1 mm, which corresponds to about 1% of the tube diameter. The numerical calculations of Schmitt et al.³ predict similar boundary-layer thickness. The turbulence levels are slightly lower than those observed in the core region.

Conclusions

The main findings of this investigation are as follows:

- 1) The flow at any given time in the cycle is nearly one-dimensional apart from thin regions near the wall boundaries. Velocity fluctuations reach a maximum peak-to-peak value of around 6% in the core region.
- 2) In all cases the boundary-layer thickness is less than 1 mm, which corresponds to about 1% of the bore. The velocity fluctuations in the boundary layer are generally lower than those in the core region.
- 3) The velocity increases linearly with axial location from zero at the breech to that of the projectile at the base.
- 4) The bulk fluid velocity scales with that of the projectile, independently of initial chamber length and pressure.

Acknowledgments

The authors are pleased to acknowledge financial support provided by the U.S. Army under contract DAJA 45-84-C-0032. Useful discussions with Dr. C. Zohani are gratefully acknowledged.

References

- ¹Krier, H. and Adams, M.J., "An Introduction to Gun Interior Ballistics and a Simplified Ballistic Code," *Progress in Astronautics and Aeronautics: Interior Ballistics of Guns*, Vol. 66, edited by H. Krier and M. Summerfield, AIAA, New York, 1979, p. 1.
- ²Giovanetti, A.J. and Rife, J.M., "Internal Ballistics Model for a Liquid Monopropellant Gun," *Journal of Ballistics*, Vol. 6, No. 1, 1982, p. 1348.

³Schmitt, J.A., Banks, N.E., Zohani, C.K., and Mann, T.L., "Two-Phase Viscous Flow Modeling of Interior Ballistics, Algorithm and Numerical Predictions for an Idealized Lagrange Gun," presented at the ASME Winter Annual Meeting, Washington, DC, Nov. 1981.

⁴Bicen, A.F., Klifas, Y., and Whitelaw, J.H., "Velocity Characteristics of the Wakes of In-Cylinder Projectiles," AIAA Paper 85-1676, 1985.

IMPERIAL COLLEGE OF SCIENCE AND TECHNOLOGY
Mechanical Engineering Department
Fluids Section, London SW7 2BX

VELOCITY CHARACTERISTICS OF THE WAKE
OF AN IN-CYLINDER PROJECTILE

by

A.F. Bicen and J.H. Whitelaw

June 1983

FS/83/19

VELOCITY CHARACTERISTICS OF THE WAKE
OF AN IN-CYLINDER PROJECTILE

A.F. Bicen and J.H. Whitelaw

Imperial College of Science & Technology, London, England

ABSTRACT

An experimental investigation of the fluid motion in the wake of an in-cylinder projectile accelerated from rest by compressed gas is reported. Time-resolved measurements of velocity were obtained by laser Doppler anemometry as a function of time and for a range of positions in the flow.

The assembly, which simulates a gun barrel, comprised a plexiglass cylinder and a flat-based projectile of 76.4 mm diameter. The initial gas pressures ranged from 1.7 to 3.8 bars and resulted in maximum projectile velocities, over a 300 mm travel, from 4.5 ms⁻¹ to 9.2 ms⁻¹. The corresponding Reynolds number range, based on cylinder diameter and atmospheric density, was 2.3 to 4.7 10⁴.

The results indicate that the flow is near one-dimensional with boundary layers generally of the order of 1% of the cylinder diameter and maximum turbulence intensities of about 4%. Velocity traces obtained near the wall boundary do not indicate turbulent fluctuations suggesting that the boundary layers remain laminar. The results also reveal that the spatial distribution of velocity between the breech and projectile base is linear at any given time in the cycle.

NOMENCLATURE

D Cylinder bore
P_i Initial chamber pressure
r_w Radial distance from cylinder wall
t Time
U Axial velocity of fluid
U_E Centreline velocity
U_p Projectile velocity
U_{pmax} Maximum projectile velocity
 \bar{u} Rms of axial velocity fluctuations

\tilde{u}/U Turbulence intensity
V_i Initial chamber volume ($\pi D^2 Z_i/4$)
Z_i Initial chamber length
z, r Cylindrical coordinates
z_p Projectile position (Z_i + z_t)
z_t Projectile travel
 δ Boundary layer thickness
 δ_d Displacement thickness
 ν Viscosity of fluid
 ρ Density of fluid

1 INTRODUCTION

The processes which take place in interior ballistics are complex and involve a continuous interaction of two phases (solid-gas or liquid-gas) through a combustion process which converts the chemical energy into heat. A number of phenomenological models have been developed, see for example reference 1 and 2, to predict these processes and subsequent projectile motion. They have, however, been inadequately tested and the need to solve problems such as tube wear requires a more detailed and assured understanding of the physical processes taking place, particularly close to the tube walls. The representation of these processes requires a multi-dimensional approach such as that of reference 3 which, in turn, requires that the physical assumptions be confirmed and quantified by experiments.

The present work is designed to provide the experimental information in the form of fluid velocity characteristics for a single-phase flow and in the absence of combustion. Although the velocities involved were an order of magnitude smaller than those found in practice, the work provides a basic understanding of the in-cylinder flow behind a projectile, directly relevant to interior

ballistics.

In the following section the test rig is described together with the experimental techniques used for projectile and fluid velocity measurements and a brief discussion on the experimental uncertainties. Results are presented and discussed in Section 3, and Section 4 summarises the more important findings.

2 EXPERIMENTAL SYSTEM

2.1 Flow Configuration

A schematic diagram of the experimental system is shown in Figure 1. The assembly was mounted vertically on a rigid table and comprised a flat-based projectile of 76.4 mm diameter, driven inside a mild steel and plexiglass cylinder of 76.7 mm diameter as indicated in Figure 1. The main regions of interest included the initial chamber and part of the volume swept by the projectile, and corresponded to the plexiglass cylinder which provided the optical access for the laser Doppler anemometer. The plexiglass cylinder was 298.3 mm in length and had a wall thickness of 12.5 mm. The clearance gap of 0.15 mm between the cylinder wall and projectile was sealed in the metal part of the cylinder by means of two silicon rubber rings as shown in Figure 1. The friction between the cylinder and projectile was kept to a minimum by PTFE guide rings lubricated by graphited grease. The total travel distance available before the projectile comes to rest was about 400 mm and a system of compression springs retarded the projectile before it has travelled this distance; this was necessary in order to reduce the impact loading on the projectile and end plate. The travel distance unaffected by the spring retardation was approximately 300 mm. The main geometric characteristics of the assembly are summarised in Table 1.

TABLE 1 GEOMETRIC CHARACTERISTICS OF THE GUN ASSEMBLY

Bore diameter, D	76.7 mm
Initial chamber length, Z _i	177.3 mm
Initial chamber volume, V _i	0.82 ltr
Maximum travel of projectile	400 mm
Unaffected travel of projectile	300 mm

The projectile was impulsively started from rest using a minimum-force-bearing release mechanism as indicated in Figure 1, and accelerated inside the

cylinder by means of initially compressed nitrogen gas at ambient temperature. The bottled nitrogen was chosen as the working fluid as it was found to be dryer than other commercially available bottled gases and as humidity, at temperatures below -80°C, causes condensation with the resulting water droplets contributing as noise-induced counts in the laser Doppler anemometry measurements. Initial gas pressures P_i were in the range of 1.7 to 3.8 bars and resulted, over the 300 mm travel, maximum projectile velocities (U_{max}) of 4.5 ms⁻¹ to 9.2 ms⁻¹. The corresponding Reynolds number range, based on the cylinder diameter and atmospheric density (U_{max} ρD/μ), was 2.3 to 4.7 10⁴.

2.2 Data Acquisition and Processing

An optical rotary encoder coupled to a gear was used in conjunction with a rack mechanism driven linearly by the projectile to determine its dynamic characteristics. The encoder provided 1000 pulses per revolution and with the particular gear diameter used (63 mm) resulted in a linear displacement of 0.2 mm per pulse. The time between two consecutive pulses were determined by a high frequency crystal clock oscillating at a rate of 1.0 MHz and values were stored in a buffer memory for subsequent processing in a microprocessor to yield the velocity-travel characteristics of the projectile.

Laser Doppler anemometry was used to obtain the fluid velocities with an optical arrangement similar to that used in reference 4. The anemometer made use of forward-scattered light and comprised a low power He-Ne laser, a focussing lens L₁, a rotating diffraction grating which splits the beam and provides the frequency shift, a collimating lens L₂, another focussing lens L₃, collecting lens L₄ and a photomultiplier which converts the optical signal into electrical signal. The principal characteristics of the optical system used are given in Table 2.

TABLE 2 PRINCIPAL CHARACTERISTICS OF THE OPTICAL SYSTEM

Half angle of beam intersection	6.1 degrees
Fringe spacing	2.98 μm
Length of probe volume at e ⁻² intensity level	0.88 mm
Diameter of probe volume at e ⁻² intensity level	62 μm

Number of fringes within e ⁻² intensity level	21
Frequency shift	1.0 MHz

Silicon oil particles were employed as light scattering particles and were obtained by using low pressure nitrogen in a blast type atomiser as described in reference 4. Particles were introduced in the initial chamber prior to the charging of the volume with the pressurised gas. The initial particle concentration obtained by this method was sufficient to obtain the measurements of time-resolved velocities at almost every part of the cylinder.

The Doppler signals from the photomultiplier output were band-pass filtered (0.2 - 5.5 MHz at -3 dB) to remove the pedestal and the high frequency noise prior to their input to a purpose-built frequency counter with a maximum sampling rate of about 22 kHz. Although there was no direction ambiguity in the fluid velocities encountered, a minimum frequency shift of 1.0 MHz was used to ensure that more than 32 fringes were present in each Doppler burst as required for efficient frequency counting, see reference 5. The input and output signals of the counter were input to an oscilloscope, as shown in Figure 1, to monitor the signal quality and to ensure its satisfactory operation during each shot. The frequency counter was interfaced to the microprocessor which sampled the digital output of the counter and stored it in the memory via a 6502 machine code at a maximum rate of 17 kHz. The time information corresponding to each frequency count was obtained from a Programmable Timer Module (PTM) which was initiated to time at a rate of 417 kHz with the arrival of the 5th encoder pulse, corresponding to the first 1 mm displacement of the projectile.

The data stored in the microprocessor and buffer memories were then processed by a software written in "BASIC" to determine both the projectile and fluid dynamics in each shot, and subsequently to plot and display them on a VDU.

2.3 Precision

For the measurements of projectile velocity a clock frequency of 1.0 MHz was used, as mentioned above, to time the projectile motion during each encoder pulse corresponding to an axial distance of 0.2 mm. Due to the count ambiguity associated with this clock frequency,

there was an inherent error in the measured projectile velocities, which increased with increasing velocity. The maximum error in the velocity range encountered was about 3%, but the overall error is expected to be much less in most parts of the cycle.

The resolution of the frequency counter is frequency dependent and for the frequency range encountered (1 - 3 MHz) corresponds, on average, to 4.7 kHz which implies a resolution of 0.014 ms⁻¹ in terms of fluid velocity. The associated error for an average fluid velocity of 3 ms⁻¹ was, therefore, less than 0.5%. The rms of the short term instability of the frequency shift was about 0.2% which implies, together with the resolution of the frequency counter, an overall error of no more than 1% in the measured velocity values.

The initial chamber pressure was read on a pressure gauge. Preliminary checks made by mercury manometers up to 1.5 bars indicated maximum deviations of less than ± 2% from the readings of the pressure gauge.

These magnitudes of the uncertainties considered above are not expected to affect the conclusions reached on the basis of the results which are presented and discussed in the following section.

3 RESULTS AND DISCUSSION

The results presented and discussed in this section are representative samples chosen to describe the flow process. Although some results are presented for maximum projectile velocities from 4.5 ms⁻¹ to 9.2 ms⁻¹ to determine the fluid velocity dependence on projectile speed, the bulk of the results pertain to maximum projectile velocity of 6.8 ms⁻¹, achieved over a 300 mm travel with the initial chamber pressure of 2.8 bars. The axial velocity traces, or values which are considered to be the predominant component of velocity, were obtained from different shots and the repeatability of experiments was generally within 1%.

Figure 2 shows typical travel-time and velocity-time curves of the projectile obtained with an initial gas pressure of 2.8 bars. The projectile velocity increases during the first 30 ms, corresponding to about 140 mm travel of the projectile, under the pressure forces exerted on its base. The velocity attains an almost constant value of about 6.8 ms⁻¹ during the next 20 ms and there-

after retards gradually as the pressure forces diminish due to expansion and the resistive forces, due to friction, take over. The abrupt fall in the projectile velocity observed after about 300 mm travel (~ 58 ms) is associated with the impingement of the projectile on the compression spring which then coils and gradually retards the projectile. The unaffected length of 300 mm travel will, therefore, be considered from now on as the projectile travel corresponding, for this particular initial pressure, to a cycle time of 56.7 ms.

The velocity-travel curves of the projectile obtained with various initial pressures ranging from 1.7 to 3.8 bars are shown in Figure 3. Increases in initial pressure result in increased projectile velocities almost in a parabolic manner as one would expect from the energy balance which neglects friction. As the sliding friction remains almost constant, the velocity-travel curves on the second half of the cycle gradually change slope from a negative value to a positive (ie from deceleration to acceleration) with increasing pressure forces as indicated in Figure 3.

The corresponding traces of centreline velocity obtained inside the initial volume and near the projectile base at $t = 0$ are shown for the gun cycle in Figure 4. The trends are similar to those of the projectile velocity and suggest that fluid velocities should scale linearly with projectile speed. This is verified by Figure 5 which indicates the linear dependence of the fluid velocity on the projectile speed obtained with different initial gas pressures. In line with the increase of overall fluid velocities, the velocity fluctuations also increase with increasing pressure and results in similar turbulence intensities (\bar{u}/U) in each case with maximum values of no more than 4%.

Figure 6 shows the centreline velocity traces at various axial locations together with the projectile velocity obtained with the initial pressure of 2.8 bars. The axial locations of $z = 100$ and 165 mm correspond to the initial chamber volume filled with gas at rest. The fluid velocities measured at these locations therefore start from zero and increase in time at a rate which approaches the projectile acceleration (dU/dt) at locations close to the base. As the projectile moves away from these locations with a continuous exchange of momentum between the fluid and the projectile, the velocities decrease in

magnitude. At locations which are initially occupied by the projectile, the fluid has a velocity equal to that of the projectile at the time it crosses this location, but the fluid subsequently lags behind the faster moving projectile with decreasing velocities in the rest of the cycle as shown in Figure 6. Although the maximum rms velocity fluctuations (\bar{u}) in the cycle increases from about 0.08 ms^{-1} at $z = 100$ mm to about 0.21 ms^{-1} at $z = 295$ mm, the intensity remains virtually the same at every location at a maximum value of about 4%. It is probable that these fluctuations stem mainly from turbulence production due to normal stresses rather than shear since, as will be shown later, insignificant velocity gradients exist in most regions of the flow. During the early part of the cycle, however, no velocity fluctuations were observed due to the stabilising effect of strongly accelerating flow.

The distributions of centreline velocity are shown in Figure 7 for various times. The most striking feature of these results is that at any given time the velocities are linearly distributed in the space between the breech and the projectile base with the values increasing from zero at the breech to that of the projectile velocity at the base. A direct implication of this result is that the linear velocity assumption widely used by interior ballisticians for the conversion of breech pressure to base pressure, see references 1 and 6 for example, is a correct one at least in the limiting case of a single-phase flow.

A description of the flow field prevailing in the gun tube during the acceleration part of the cycle is given in Figure 8 which presents the radial profiles of axial velocity at various times and axial locations. The profiles reveal that the velocities increase with time and axial location, and that they are uniformly distributed across the cylinder indicating that the flow is one-dimensional throughout the space and cycle apart from the thin regions near the wall boundaries.

More detail of the flow near the wall boundaries at $z = D$ (76.7 mm) and $2D$ (153.4 mm) is given in Figures 9 and 10 respectively, which presents the velocity traces at radial distances r of 0.5, 1, 2 and 3 mm away from the wall. These traces do not show any significant enhancement in velocity fluctuations near the wall boundary and suggest that the boundary layers are laminar and remain laminar throughout the cycle. The velocity values at $r = 0.5$ mm are generally of the order of 95% of the

velocities at $r = 3$ mm and suggest that the boundary layer thickness δ is less than 1 mm corresponding to about 1% of the cylinder diameter. The calculations of reference 3 based on laminar flow indicate that the displacement thickness δ^* , which is roughly 30% of the boundary layer thickness (see for example reference 7), is generally of the order of about 0.3% of the diameter corresponding therefore to similar boundary layer thicknesses to those observed here.

4 CONCLUSIONS

The main findings of this investigation can be summarised as follows:

1. The flow at any given time in the cycle is near one-dimensional and laminar with velocity fluctuations corresponding to maximum intensities of about 4%.
2. The boundary layers remain laminar during the cycle and correspond to about 1% of the cylinder diameter.
3. The fluid velocities are linearly distributed in the space between the breech and projectile base with velocities increasing from zero at the breech to that of the projectile near the base.
4. The fluid velocities show a linear dependence on the projectile speed obtained with different initial gas pressures.

ACKNOWLEDGEMENTS

The authors would like to acknowledge the financial support provided by the U.S. Army Research Office. They would also like to thank Mr J Laker for his contribution in electronic hardware and Mr N Frost for the construction of the experimental rig.

REFERENCES

1. Krier H and Adams M J, "An Introduction to Gun Interior Ballistics and a Simplified Ballistic Code", Progress in Astronautics and Aeronautics, Edited by Krier H and Summerfield M, AIAA, Vol.66, p.1, 1979.

2. Giovanetti A J and Rife J M, "Internal Ballistics Model for a Liquid Monopropellant Gun", Journal of Ballistics, Vol.6, No.1, p.1348, 1982.
3. Schmitt J A, Banks N E, Zoltani C K and Mann T L, "Two-Phase Viscous Flow Modeling of Interior Ballistics, Algorithm and Numerical Predictions for an Idealized Lagrange Gun", Presented at the ASME Winter Annual Meeting, Washington D.C., Nov. 1981.
4. Bicen A F, "Air Flow Characteristics of Model Internal-Combustion Engines", Ph.D. Thesis, University of London, 1983.
5. Founti M A and Laker J R, "Performance of a New Frequency Counter Interfaced to a Micro-processor Controlled Data Acquisition and Processing System", Imperial College, Mech. Eng. Dept. Report FS/81/36, 1981.
6. Campbell A S, "Thermodynamic Analysis of Combustion Engines", John Wiley & Sons, 1979.
7. Schlichting H, "Boundary-Layer Theory", McGraw-Hill, Sixth Edition, 1968.

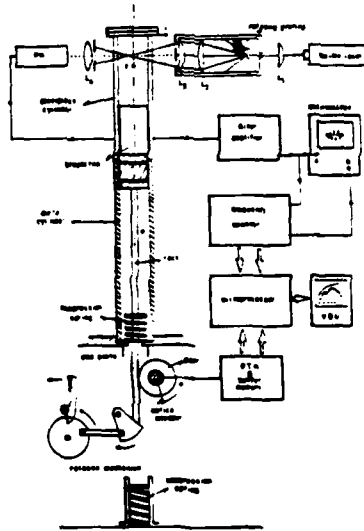


Figure 1 Schematic of Experimental System

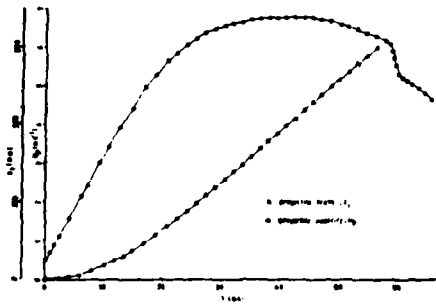


Figure 2 Travel-time and velocity-time curves of projectile

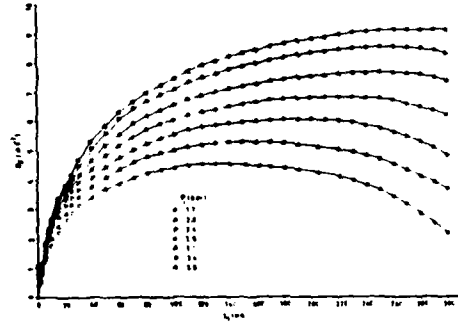


Figure 3 Velocity-travel curves of projectile for various initial pressures

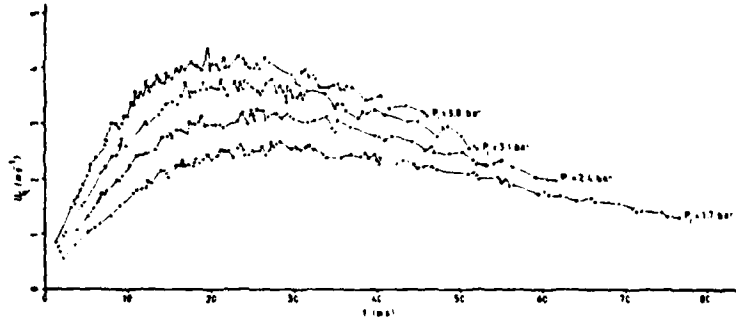


Figure 4 Centreline velocity traces at $z = 165$ mm for various initial pressures

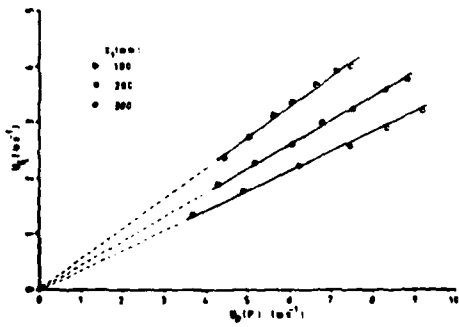


Figure 5 Fluid velocity dependence on projectile speed, centreline velocities at $z = 165$ mm

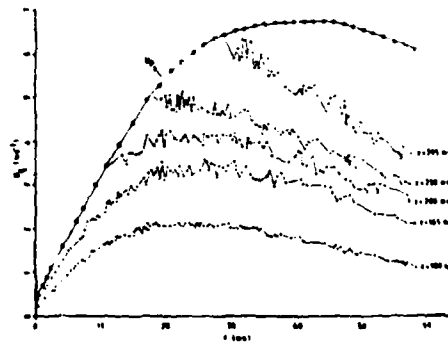


Figure 6 Centreline velocity traces at various axial locations

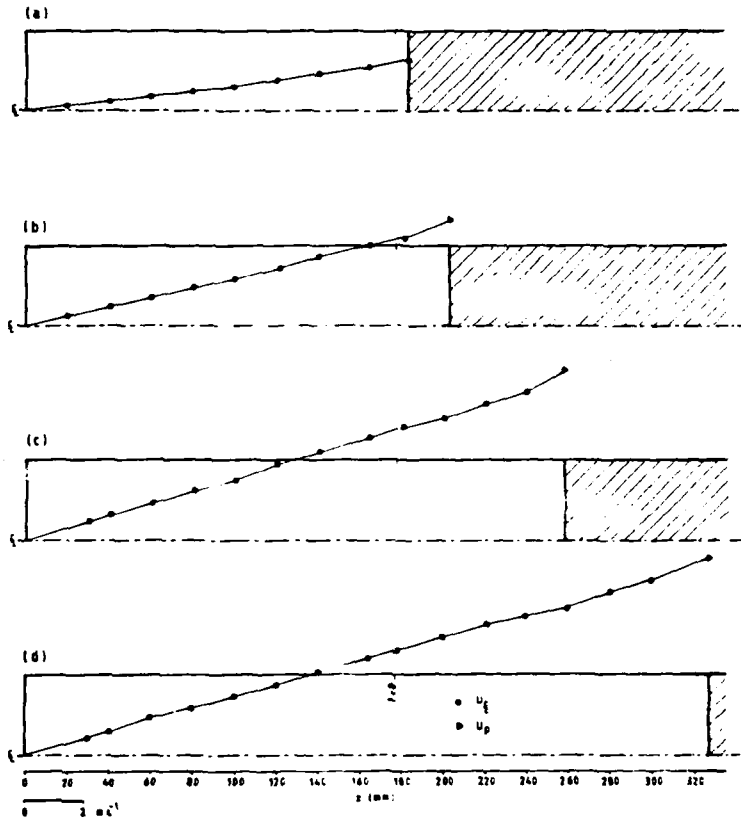


Figure 7 Centreline velocity distribution at various times in the cycle.
 (a) $t = 4.8$ ms (b) $t = 11.6$ ms (c) $t = 22.8$ ms
 (d) $t = 33.8$ ms

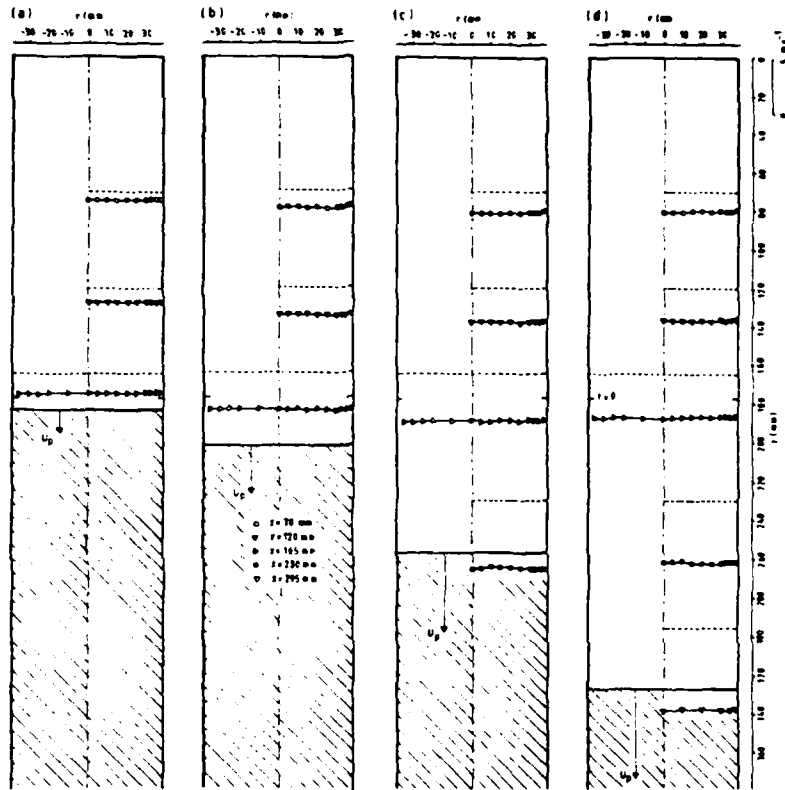


Figure 8 Radial distributions of velocity at various times in the cycle. (a) $t = 4.8$ ms (b) $t = 11.6$ ms (c) $t = 22.8$ ms (d) $t = 33.8$ ms

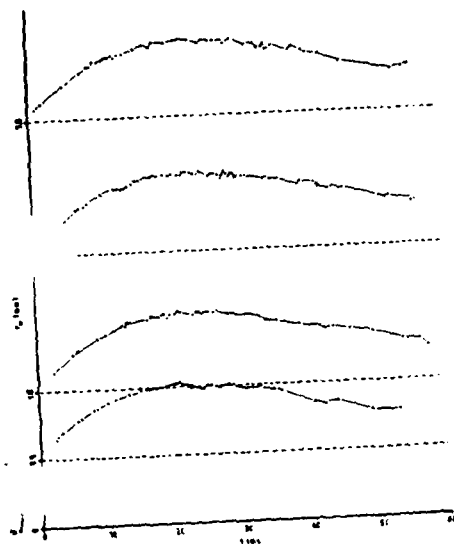


Figure 9 Velocity traces near wall boundary at $z = D$ (76.7 mm)

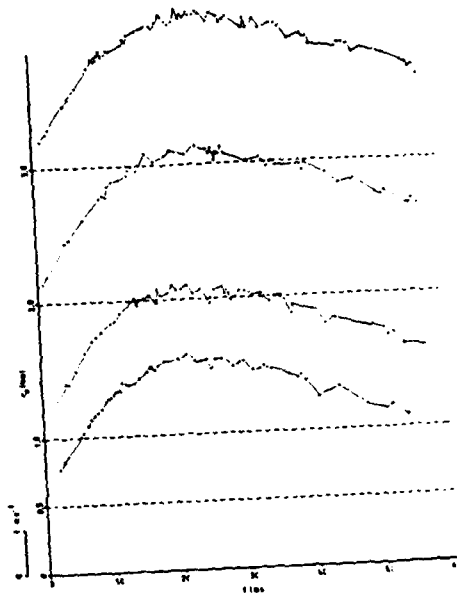


Figure 10 Velocity traces near wall boundary at $z = 2D$ (153.4 mm)

IMPERIAL COLLEGE OF SCIENCE AND TECHNOLOGY
MECHANICAL ENGINEERING DEPARTMENT
Exhibition Road, London SW7 2BX

SUBSONIC SINGLE-PHASE FLOW IN A GUN SIMULATOR

by

A F BICEN, L KHEZZAR and J H WHITELAW

Submitted to AIAA Journal, September 1986

ABSTRACT

Time-resolved and ensemble mean and rms fluid velocities obtained by laser Doppler anemometry in a subsonic gun simulator with an inert/single-phase flow and a projectile exit velocity of 40m/s are reported. The results presented also include the time-resolved measurements of projectile velocity and breech pressure.

The results show that the calculated projectile velocities based on measured breech-pressure record are almost exactly equal to the measured values and confirm that the friction of the system is negligible. Fluid velocity traces, together with ensemble mean and rms velocity profiles, indicate the presence of a wall boundary layer which occupies up to 20% of the tube radius and with a growth rate similar to steady turbulent boundary layers. The nature of velocity fluctuations and the shape of velocity profiles inside the boundary layer also suggest that the boundary layers in the wake of the projectile are turbulent.

LIST OF SYMBOLS

A	cross-section area of projectile
a	local speed of sound
d	tube diameter
F_r	friction force
g	acceleration of gravity
m	mass of projectile
P_a	atmospheric pressure (back pressure)
P_b	breech pressure
P_o	absolute initial pressure
R	tube radius
r	distance from cylinder wall
t	time
U	ensemble mean axial velocity
U_c	centreline mean velocity
u'	ensemble rms axial velocity
V_p	projectile velocity
x	Eulerian coordinate measured from breech (fluid)
z	Lagrangian coordinate (projectile)
z_o	initial chamber length
γ	isentropic coefficient
δ	boundary layer thickness
ρ_o	initial fluid density

1. INTRODUCTION

The flow field behind the projectile in a real gun is characterized by high velocities of solid and gas phases and by exothermic reactions, with temperatures up to 3000 K, reference 1, and unsteady boundary layers at the walls behind the projectile. The short duration of the projectile travel within the barrel adds to the difficulty of accurate measurements of the high speed transient phenomena. A related program of research has recently been recommended, reference 2, and involves experiments with simulators that permit the generation of well controlled flows, starting with more simplified single-phase inert flows and advancing progressively towards more complex two-phase reacting flows. A strong interest is also being shown by computational communities (references 3 and 4) which, it is hoped, will provide means of interpolation and extrapolation of the experimental results. Heiser (reference 4), for example, has obtained encouraging agreement with the experimental results of reference 5, by solving the full Navier-Stokes equations for laminar flows.

The work presented here describes inert single-phase measurements of pressure, projectile and fluid velocities in a subsonic gun simulator. The model gun is of the preburned-propellant and constant-diameter type, in ballistic phraseology. It constitutes a continuation and improvement of the work reported in reference 5. The wall shear layers which existed in a gas expanding behind a projectile of reference 5 were found to be less than 1% of the tube diameter and it was difficult to provide detailed results which would clarify the nature of the unsteady boundary layer. In the present study the length of the travel of the projectile has been extended thus allowing the boundary layers to grow more than previously. Little is known about transient boundary layers (references 6 and 7) and, consequently, particular attention is paid to the nature of the ensuing boundary layers since their behaviour accounts for momentum and heat transfer to

the wall of the barrel. In addition, a novel optical technique has been developed and used successfully to obtain the projectile velocity as a function of space and time. This work also represents a stage in a program of research aimed at measuring in high-speed two-phase flow configurations by evaluating measurement techniques.

2. EXPERIMENTAL TECHNIQUES

2.1 Flow configuration

The flow arrangement shown in Figure 1 is similar to that in reference 5 but has a projectile travel of $14d$ as opposed to $4d$ and a lighter projectile to achieve higher velocities with the range of initial pressures previously used.

The projectile is secured in position inside a tube of 76.5mm diameter which is pressurized by compressed nitrogen. After the gas becomes quiescent, the projectile is released and travels a distance of about $1m$ ($\approx 13d$) inside the tube which is machined to high precision. The initial chamber of 306mm ($4d$) in length is fabricated from plexiglass to provide optical access for the laser Doppler anemometer. The remainder of the barrel is made of mild steel, with four small circular plexiglass windows, as shown in Figure 1, to allow velocity measurements at axial distances of approximately 7 , 10 , 13 and $16d$ from the breech. A lock mechanism has been designed to secure the projectile under the pressure load at its starting position and to release it smoothly and spontaneously without causing jitter. The initial sealing of the chamber is achieved by means of an O-ring fitted around the inner surface of the tube, against which the projectile rests at its start position. After the projectile is released and during its travel inside the barrel two plastic

rings fitted on the projectile prevent blow-by of the compressed gas. The projectile is 250mm long and weighs 0.953kg. The top and bottom parts are made of aluminium alloy and a central plexiglass section houses a linear graticule for projectile velocity measurements. At the end of its travel, the projectile is decelerated by compression of the air inside the lower part of the barrel. A control valve fitted at the bottom and connected to a compressed air supply is used to return the projectile to its lock and start position at the top of the barrel.

2.2 Measurement systems

Emphasis has been placed on the development of an improved method for measuring the projectile velocity. The chosen optical technique makes use of a linear graticule and eliminates the need for the alternative and mechanically complex rack and gear mechanism of reference 5 and removes the ambiguity in the associated friction force. The graticule inside the projectile consists of 25 lines per inch. The measuring systems are shown in Figure 1.

For the projectile velocity measurements, the instrumentation comprises a 5mW He-Ne laser, a lens to focus the beam at its waist on the graticule, a pinhole and another lens to focus the emerging beam onto a photodiode. The lens-pinhole combination reduces the field of view of the diode to a minimum possible for the system operation and thereby reduces the sensitivity of the system to unwanted optical noise from reflections and flares. The graticule moves with the projectile and transmits a pulse train whose period coincides with the chopping of the laser beam by the graticule. The output signal of the diode is converted to a square wave by a schmitt trigger, which is compatible with

digital logic. The individual periods are timed by a high frequency clock and stored in a buffer memory from which the velocity of the projectile can be computed during the part of the cycle corresponding to the transient time of the projectile across the selected window. By repeating the measurements at each of the four windows, velocity-travel curve for the whole cycle can be assembled.

For the measurements of fluid velocity a dual-beam laser Doppler anemometer operated in the forward-scatter mode was used. The anemometer consisted of a 32mW He-Ne laser, a focussing lens, a rotating diffraction grating, a collimating lens, a collecting lens and a photomultiplier as also shown in Figure 1. The principal characteristics of the optical system are given in Table 1. Silicone oil particles were

TABLE 1 Principal characteristics of optical system

Half angle of intersection of beams	6.10 degrees
Fringe spacing	2.99 μm
Length of probe volume at e^{-2} intensity level	0.908 mm
Diameter of probe volume at e^{-2} intensity level	0.097 mm
Number of fringes within e^{-2} intensity level	34

used as scattering particles and were introduced in the initial chamber prior to charging of the volume at the required release pressure. The output of the photomultiplier was band-pass filtered to remove the pedestal and the high frequency noise and input to a purpose built frequency counter with an 8/16 validation logic and a cycle time of 45 μsec . The frequency counter was

interfaced to a microcomputer which sampled the digital output of the counter and stored it in memory at a rate of $\approx 10\text{KHz}$. The time information corresponding to each frequency count was obtained from a programmable timer module which was activated to time at a rate of 477KHz after the first 2mm of the projectile travel. The data was subsequently processed by the microcomputer to determine and display the variation of velocity as a function of time.

The initial pressure used was 8 bars and achieved with low grade nitrogen taken from a pressurised cylinder. The initial pressure and the breech pressure record during the cycle were measured with a precision of ± 0.002 bars, using a piezoelectric transducer and a charge amplifier whose analogue output was digitized and interfaced with the microcomputer.

3. RESULTS AND DISCUSSION

3.1 Projectile dynamics

Figure 2 shows the measured velocity-travel curve of the projectile together with the curve calculated from the measured breech pressure-time record. The measured traces were found to be repeatable within 1% from cycle to cycle over a large number of cycles and the problem of varying friction encountered with the previous experimental set-up of reference 5 has been removed. The projectile accelerates rapidly from rest to reach its exit velocity of about 40m/s in about 30msec . The acceleration of the projectile is greatest at the start of the motion and decreases monotonically to reach almost zero at the end of the cycle.

The motion of the projectile can be determined if the pressure acting on its base is known. The relation that

gives the base pressure as a function of the breech pressure acting along a characteristic line is (reference 8):

$$P_{\text{base}} = P_{\text{breech}} \cdot \left(1 - \frac{\gamma-1}{2} \cdot \frac{V_p^{2\gamma/\gamma-1}}{a}\right) \quad (1)$$

The projectile motion as a function of the breech pressure is then given by the equations:

$$\begin{aligned} \frac{dv_p}{dt} = & A \cdot m^{-1} \cdot P_b \cdot \left\{1 - \frac{\gamma-1}{2} \cdot \frac{V_p}{\rho_0} \left(\frac{\gamma}{P_b}\right)^{\gamma-1/\gamma} \cdot P_0^{1/\gamma}\right\}^{2\gamma/\gamma-1} \\ & - P_a \cdot A \cdot m^{-1} + g + F_r \cdot m^{-1} \end{aligned} \quad (2)$$

$$v_p = \frac{dz}{dt} \quad (3)$$

In equation 2 the compressibility effect on the atmospheric side has been ignored since under the present conditions it does not contribute more than 0.5% to the exit projectile velocity (see reference 9 for example). Preliminary pressure measurements obtained near the muzzle verified this assumption.

Equations 2 and 3 constitute a coupled set of simultaneous ordinary differential equations in z and V_p in terms of t and can be solved numerically, by a standard fourth order Runge-Kutta Algorithm. The friction force term in Equation 2 is taken to be equal to zero since no a priori model for it exists. The calculated values for V_p in Figure 2 indicate a value at the exit position of 40.0m/s which is almost exactly equal to the measured value and thus suggests a negligible friction force. This fact assumes particular significance for numerical predictions, which obviates the need for considerations of the wall friction force.

3.2 Fluid velocity measurements

The centreline velocity traces of the fluid together with the projectile velocity measurements are shown in Figure 3 for the axial stations of $x = 3d$, $x = 7.27d$, $x = 10.20d$, $x = 13.13d$ and $x = 16.07d$. At $x = 3d$, which corresponds to the position inside the initial chamber, the fluid velocity increases monotonically with time to reach a maximum of 14m/s at around 10msec. During the acceleration period no fluctuations are present. The velocity, after reaching the maximum, decreases to 7m/s on average at about 35msec and fluctuations, though of low magnitude, start to appear with decreasing acceleration. The fluid velocities immediately behind the projectile have been measured at subsequent axial stations and increase in accord with the projectile velocity which forms an envelope to the fluid velocities. At these axial stations, the fluid velocities decay in an almost linear fashion with time, as the projectile moves away. The fluctuations increase with axial distance.

Figure 4 shows fluid velocity traces at $x = 7.27d$ for different radial positions from the wall and suggests that fluid is turbulent and certainly far from laminar. All radial positions reveal similar decay in almost linear fashion with time. The fluid velocities at 13msec are almost the same as the corresponding projectile velocity of 30m/s as expected. As the wall is approached, the relative magnitude of the fluctuations increases and fewer velocity values are recorded. This suggests that the density of scattering particles is lower than in the core of the flow. It can also be seen that the mean level of the instantaneous velocities drops close to the wall.

In order to build a picture of the flow inside the barrel at a certain time, ensemble mean and rms values need to be considered during a finite time interval and over many single realizations. The experimental sample size was chosen

to be greater than 80 within a time interval of 3msec as a compromise between the need to reduce the time gradient broadening and the number of samples necessary to obtain an acceptable statistical error. The number of at least 80 samples ensured a maximum statistical error, according to reference 10, in the mean velocity of 2%. In the core of the flow where the sample sizes were generally greater than 120, the error is less than 1%. The corresponding error in the rms velocity is of the order of 10%.

Other sources of error are gradient broadenings due to the variation of the velocity within the averaging time interval of 3msec and within the measuring probe volume. The maximum possible error including the accuracy of the measurement system, gradient broadenings and the statistical uncertainty is about 4% in the mean velocity and less than 20% in the rms velocity.

Figure 5 presents radial profiles of the mean and rms axial velocity inside the barrel for a time of 26msec at $x = 7.27d$, $x = 10.20d$ and $x = 13.13d$ and represents the state of the fluid motion when the projectile has almost reached the muzzle. The mean velocity profiles show similar trends, with a flat core which occupies almost 80% of the barrel radius. Near the wall both mean and rms profiles reveal the existence of a shear layer. The rms values are low over the bulk of the flow, around 4% of the local mean velocity, and increase to reach 10% of the mean velocity near the wall. Also shown in Figure 5 is the axial distribution of the boundary layer thickness, which increases from 0.18R at $x = 7.27d$ to 0.21R at $x = 10.20d$ and decreases to 0.15R at $x = 13.13d$ and should go to zero at the projectile base.

Little is known about the behaviour of transient boundary layers and a comparison with steady boundary layers may be helpful. Figure 6a shows the variation of the measured boundary layer thickness with axial distance at a fixed time

of 26 msec together with the calculated variations of a steady incompressible laminar boundary layer starting at the breech and steady incompressible turbulent boundary layers with zero and favourable pressure gradient (reference 11), starting at the end of the initial chamber where the boundary layers are believed to be laminar, reference 5. For the calculations of boundary layer thickness with favourable pressure gradient, a linear variation of core velocity between the breech and projectile base was used at the chosen time to evaluate the corresponding pressure gradient. The measured boundary layer thicknesses are more closely related to the turbulent boundary layers as shown in the figure.

Figure 6b shows the measured velocity profiles inside the boundary layer for different times and axial locations, together with 1/7-power law of turbulent steady flow inside a tube. The measured velocity profiles follow closely the 1/7-power law. The exponent for the measured profiles can be found by the least-squares technique which give values from 1/6.6 for the lowest bulk Reynolds number based on the diameter of the tube, which occurs at the earliest parts of the projectile motion to 1/9.9 for the highest bulk Reynolds number which occurs when the projectile reaches the muzzle. The calculated shape factor ranged from 1.2 to 1.3 and again suggests that the measured boundary layers are turbulent (reference 12).

Figure 7 shows the profiles of the mean axial velocity at $x = 7.27d$ for three different times during the cycle of 14.5, 26 and 30.5msec and represents the evolution of the mean axial flow with time at a fixed position (Eulerian frame). It can be seen that the boundary layer thickness increases from 0.12R at 14.5msec to reach 0.19R later in the cycle. The boundary layer at a fixed position, therefore, grows with time during the cycle and reaches an almost constant thickness. Figure 8 shows the evolution of the mean and rms axial velocity profiles at a fixed location of 60mm behind the moving projectile, so that it represents the flow following the motion of the projectile (Lagrangian frame). In common with Figure 7, the profiles at 14.5msec show a boundary layer thickness of 0.12R which grows, however,

at a much slower rate to reach 0.13R at 20.5msec and 0.15R at 26msec.

4. CONCLUSIONS

The following main conclusions may be extracted from the preceding text:

1. The relationship between the breech pressure and the projectile velocity may be determined by consideration of one-dimensional, unsteady forms of the continuity and momentum equations. The measured breech pressure record leads to calculated projectile velocity values within 0.5% of the measured ones and confirms that the friction between the projectile and the tube wall is negligible.

2. The fluid velocity traces, together with the corresponding ensemble mean and rms velocity profiles, indicate the presence of a shear layer which exists behind the projectile and occupies around 20% of the tube radius. In the initial chamber, the boundary layer thickness is of the order of 1% of the radius.

3. The nature of the fluid velocity fluctuations and the shape of the ensemble mean and rms velocity profiles inside the boundary layer, suggest that the boundary layer is turbulent. The evolution of the boundary layer thickness as compared to steady turbulent and laminar boundary layers shows that it is closer to the former.

ACKNOWLEDGEMENT

Financial support provided by the US Army and the Atomic Energy Research Establishment at Harwell is gratefully acknowledged. The technical assistance of Messrs J Laker and P Trowell is also appreciated.

REFERENCES

1. C L Farrar & D W Leeming "Military Ballistics, a Basic Manual", Brassey's Defence Publishers, 1983
2. G Klingenberg & N E Banks "Review on interior and transitional ballistic research: state of the art of computational and experimental efforts", EMI Report Expl - Nr 028, 1981
3. J A Schmitt, N E Banks, C K Zoltani & T L Mann "Two-phase viscous flow modelling of interior ballistics, algorithm and numerical predictions of an idealized Lagrange gun", presented at ASME Winter Annual Meeting, Washington DC, Nov. 1981
4. R Heiser "Two-phase flow, interior ballistic modelling", US Army Workshop of two-phase flows, Imperial College Mech. Eng. Dept., Fluids Section, London, Nov. 1985
5. A F Bicen, Y Kliafas & J H Whitelaw "In-bore velocity measurements in the wake of a subsonic projectile", AIAA Journal, v. 24, p. 1035, 1986
6. W J McCroskey "Some current research on unsteady fluid dynamics", Journal of Fluid Engineering, v. 99, 1976

7. L W Carr "A Review of Unsteady Turbulent Boundary Layer Experiments, in Unsteady Turbulent Shear Flows", Ed. by R Michel, J Cousteix and R Houdeville IUTAM Symposium, Toulouse, 1981
8. A A Shapiro "The Dynamics and Thermodynamics of Compressible Fluid Flow", Ronald Press Co, New York, v. 2, 1953
9. A E Seigel "Theory of High-Muzzle-Velocity Guns, Interior Ballistics of Guns", Edited by H Krier & M Summerfield, Progress in Astronautics and Aeronautics, v. 66, p. 135, 1979
10. W J Yanta & R A Smith "Measurements of turbulence - transport properties with a laser Doppler velocimeter", AIAA Paper no. 73-169, AIAA 11th Aerospace Science Meeting, Washington, 1978
11. W M Kays & M E Crawford "Convective Heat and Mass Transfer", McGraw-Hill, 1980
12. H Schlichting "Boundary Layer Theory", McGraw-Hill, 7th Edition, 1979

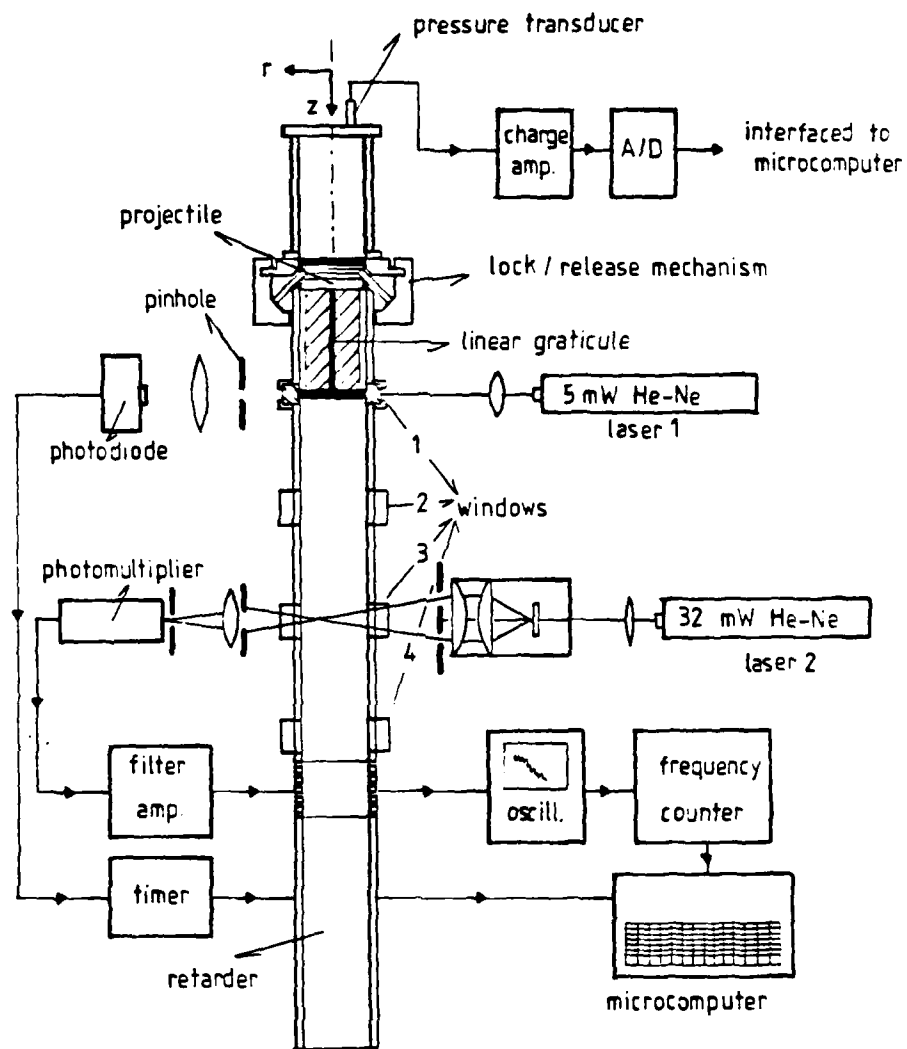


Figure 1: Schematic diagram of experimental set up

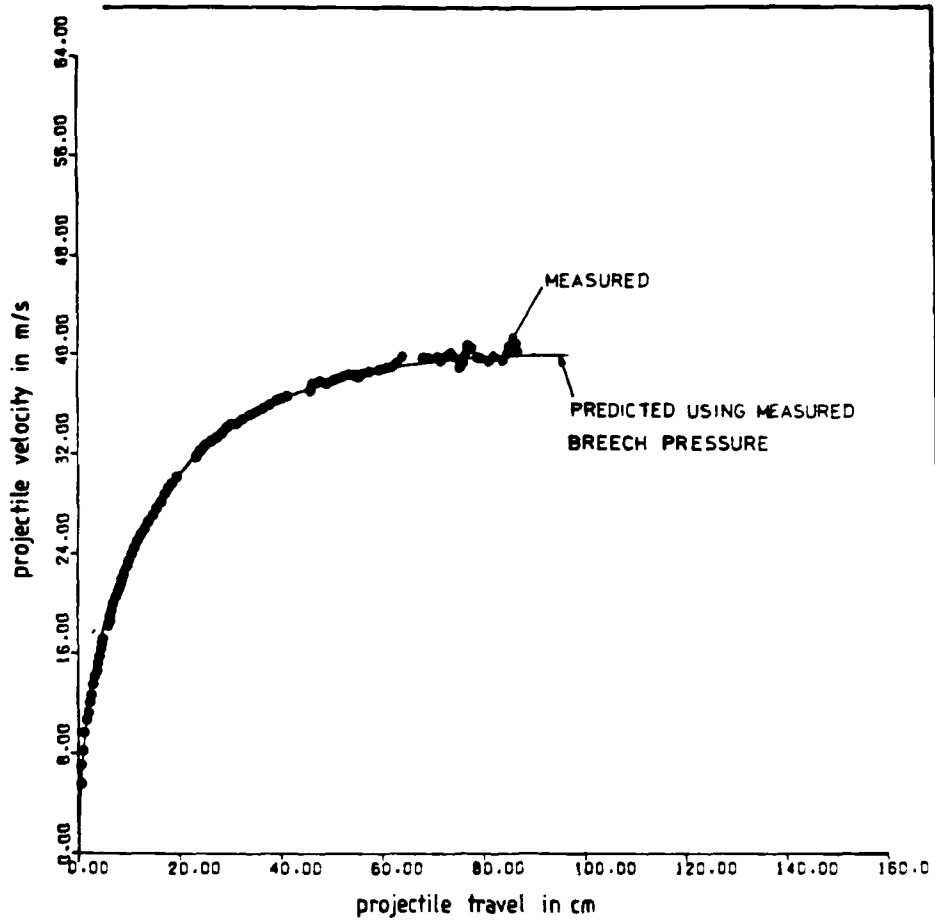


Figure 2: Measured and predicted projectile velocity-travel curves

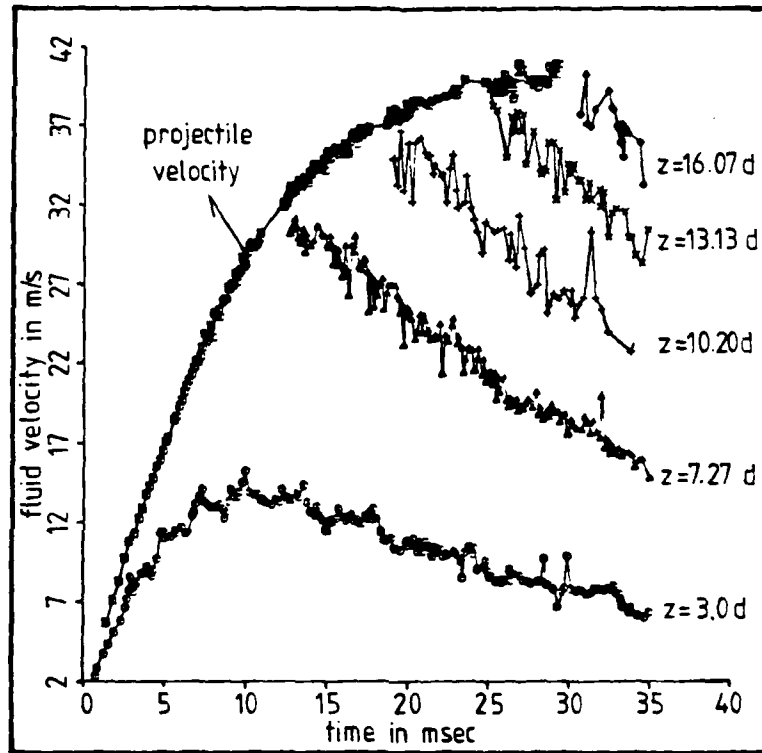


Figure 3: Centreline velocity traces at different axial stations

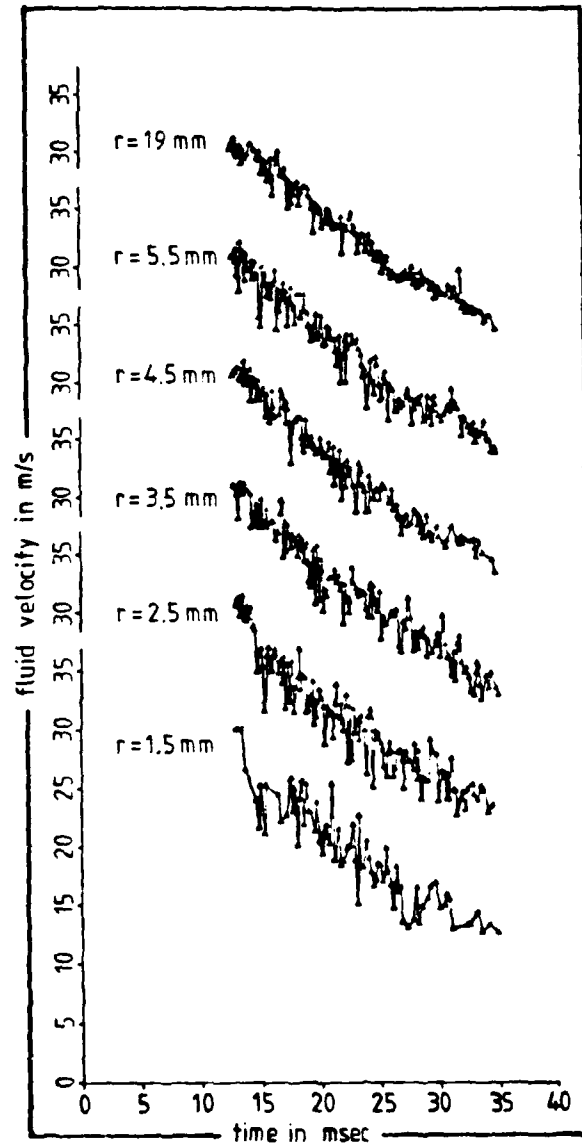


Figure 4: Fluid velocity traces at $x = 7.27d$ for different radial positions from the wall

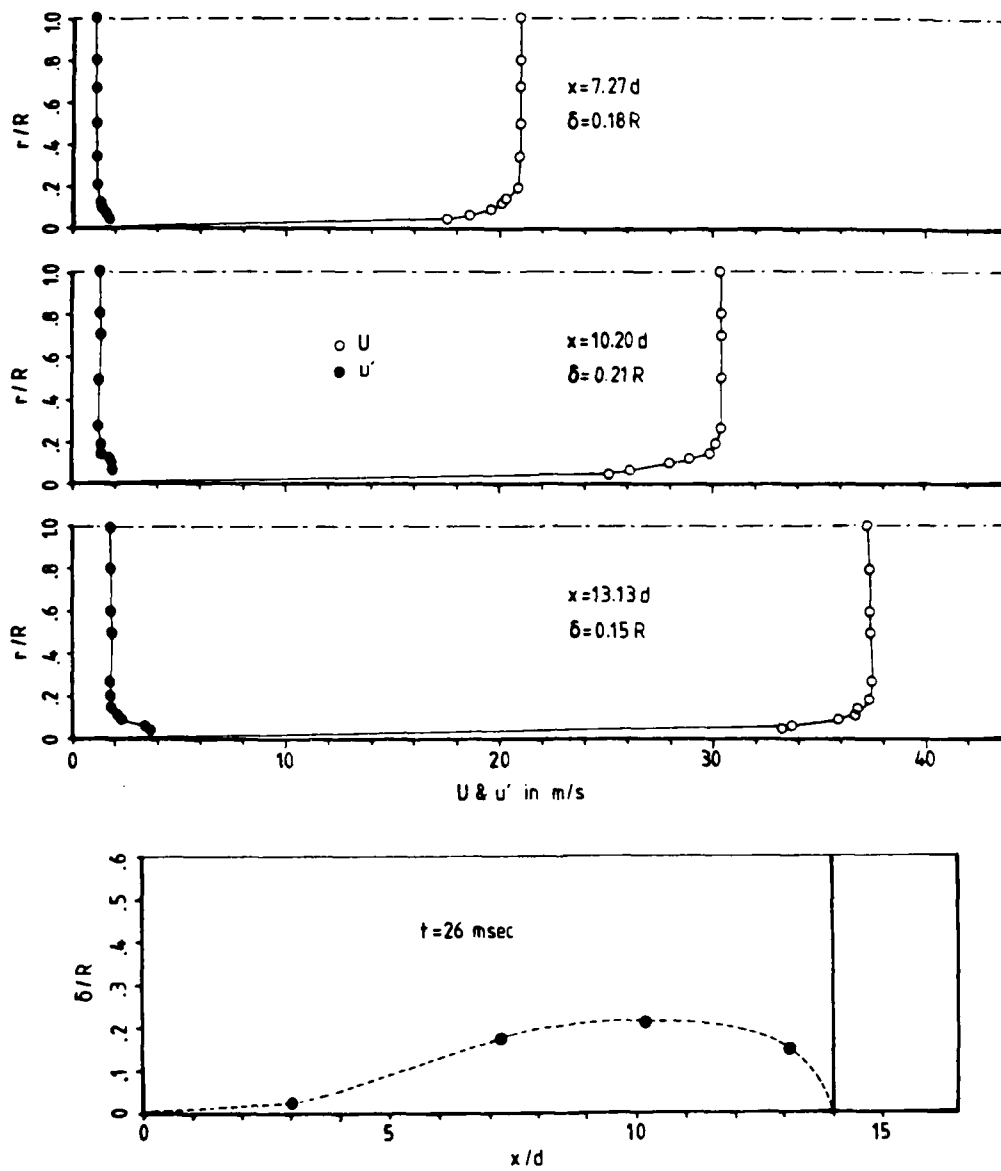


Figure 5: Mean and rms velocity profiles at $t = 26$ msec for $x = 7.27d$, $x = 10.20d$ and $x = 13.13d$.

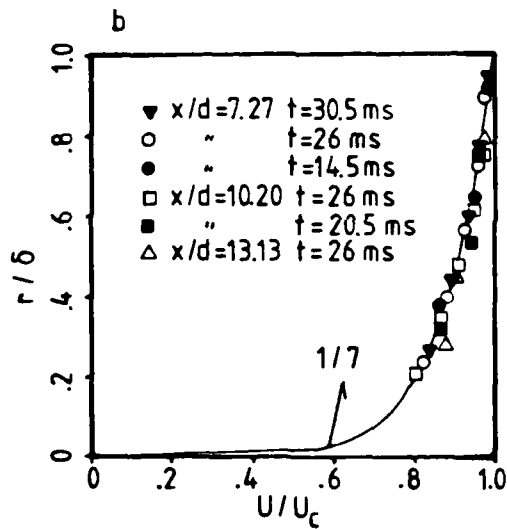
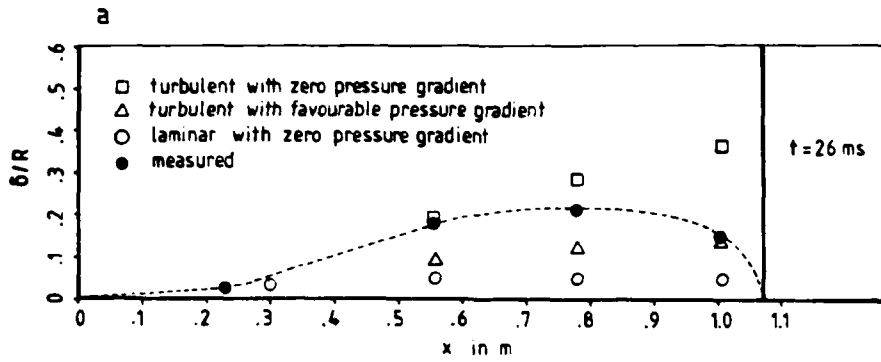


Figure 6: (a) Measured and calculated steady boundary layer thicknesses
 (b) Velocity distribution inside the boundary layer; the line represents the 1/7-power law

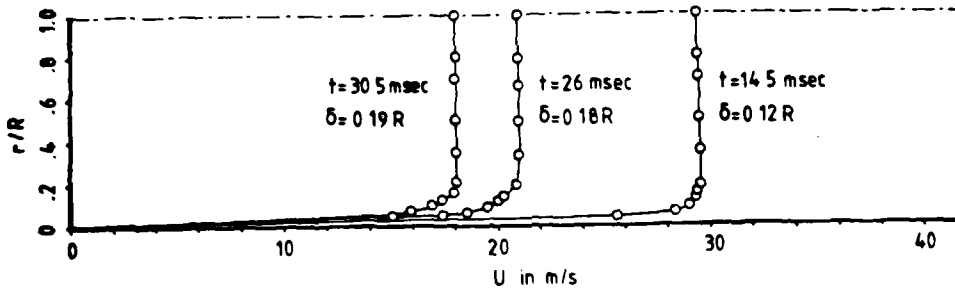


Figure 7: Mean velocity profiles at $x = 7.27d$ for different times

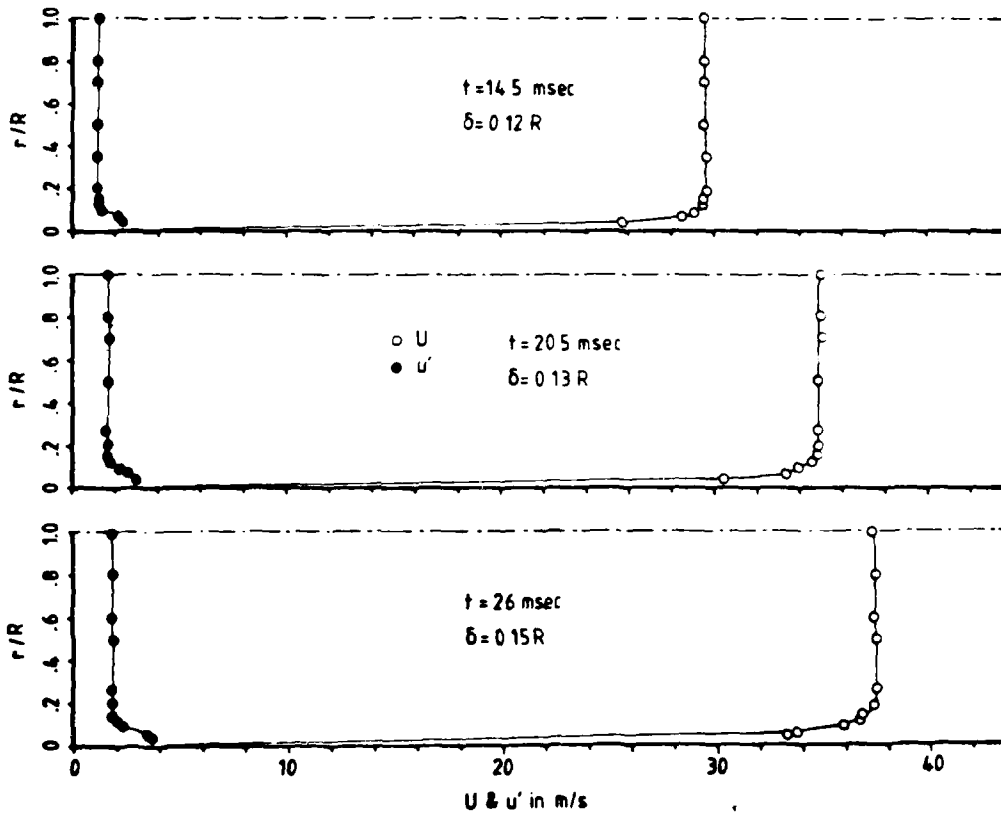


Figure 8: Mean and rms velocity profiles at $x = z + z_0 - 60\text{mm}$ for different times

IMPERIAL COLLEGE OF SCIENCE AND TECHNOLOGY
Fluids Section, Department of Mechanical Engineering
Exhibition Road, London SW7 2EX, England.

SUBSONIC SINGLE- AND TWO-PHASE FLOW CHARACTERISTICS OF A GUN SIMULATOR

by

A F Bicen, L Khezzar and J E Whitelaw

Semi-annual report for
Contract DAJA-45-84-C-0032

September 1986

FS/86/43

Abstract

Fluid and solid particles (500 μm diameter) velocities obtained by laser Doppler anemometry in a subsonic gun simulator with inert single- and two-phase flow are reported. The gun simulator is of the preburned propellant chambered type with a gradual contraction in the top initial chamber which incorporated a particle injector mechanism. The results show that the effect of the chambered geometry on fluid and projectile velocity and on the growth of the wall shear layer remained negligible within the subsonic range considered. Comparison between the velocity of 500 μm Diakon particles and that of the fluid obtained separately in the absence of solid particles revealed that the particles lag behind the fluid in regions closer to the projectile because of their relatively large inertia, and that the lag increases with axial distance from the breech reaching a measured maximum of about 2% near the end of the cycle. The observed rms levels of particle velocity are higher than those of the fluid in the bulk of the flow but attain similar values near the tube wall.

Abstract

1. Introduction
2. Experimental System
3. Results and Discussion
 - 3.1 Projectile dynamics
 - 3.2 Single-phase flow
 - 3.3 Two-phase flow
4. Conclusions

Acknowledgement

References

Figures

1. Introduction

In a real gun environment, the interior ballistic flow is transient and reactive with fast burning propellant grains, metal and soot particles of various sizes and of irregular shapes. The two-phase nature of the flow adds to its complexity and makes it almost impossible to probe the flow for velocity information. Progress in modelling and calculation methods (1, 2), on the other hand, calls for understanding of the characteristics of unsteady, two-phase flows in relevant arrangements, and the corresponding measurement problems imply that simplified geometries are required.

The flowfield behind a moving projectile in a single-phase subsonic gun simulator has been quantified (3, 4) and the related transient boundary layers were shown to be similar to steady turbulent boundary layers. This paper reports experiments with inert single- and two-phase flows in a similar gun simulator and represents a further step towards reality. The single-phase flow experiments quantify the effect of initial chamber geometry including a gradual contraction similar to those of real gun systems and the two-phase flow results quantify the behavior of 500 μm Diakon particles. The latter make use of a particle-injector mechanism fitted to the breech chamber to introduce the monodispersed particles with initial volume concentration of about 1.3%.

The following section describes the gun simulator and the experimental techniques. Section 3 presents and discusses the results and Section 4 summarizes the main findings of this work.

2. Experimental System

A diagram of the gun simulator, which is mounted vertically, is shown in Figure 1 and is similar to that of (3), with the exception of the initial chamber geometry which comprises a gradual contraction from a diameter of 150 mm to 76.5 mm. The initial chamber of (3) had a constant diameter of 76.5 mm and approximately the same volume. The

present arrangement simulates more closely the initial chamber geometry of real gun systems (5) and incorporated a 13 mm thick disk, with twelve 14 mm-diameter holes distributed as shown on figure 1, and initially filled with 500 μ m Diakon particles. The holes were sealed by spring-loaded cones pushed against them by the projectile in its lock position. On release of the projectile, the cones retracted and the particles entered the initial chamber. The number of holes, their distribution, cone angle and the particular initial chamber geometry were chosen to cause the particle distribution in the initial volume to be as uniform as possible. The volume above the disk was less than 5% of the total initial volume with consequently small jet momentum. With this arrangement an initial particle concentration of up to 1.3% by volume was achieved and corresponded to a mass loading of about 2.3.

The projectile was secured in position at the top of the barrel by a lock/release mechanism as shown in Figure 1, and the initial chamber pressurised by compressed nitrogen. After the gas became quiescent, the projectile was released and the particles injected. The projectile travelled a distance of about 1 m inside the 76.5 mm diameter tube which was machined to high precision and contained four small plexiglass windows to provide optical access for laser Doppler anemometry measurements at axial locations of approximately 5d, 8d, 11d and 14d from the breech. The initial sealing of the chamber was achieved by means of an O-ring fitted around the inner surface of the tube against which the projectile rested at its start position. After the projectile was released and during its travel inside the tube, two PTFE-rings fitted to the projectile prevented blow-by of the compressed gas. The projectile was 250 mm in length and weighed 0.953 kg. The top and bottom parts were made from aluminium alloy and the central plexiglass section housed a linear graticule with 25 lines per inch for projectile velocity measurements. At the end of its travel, the projectile was decelerated by the compression of air inside the lower part of the barrel. A control valve fitted at the bottom and connected to a compressed air supply was used to return the projectile to its lock and start position at the top of the barrel.

The projectile velocity was measured with the optical system of Figure 2 and comprised a 5 mW He-Ne laser, a lens to focus the beam at its waist on the graticule, a pinhole and a second lens to focus the emerging beam onto a photodiode. The graticule moved with the projectile and transmitted a pulse train whose period coincided with the chopping of the laser beam by the graticule. The individual periods were timed by a high frequency clock and stored in a buffer memory and the projectile velocity computed during the part of the cycle corresponding to the transit time of the projectile across the selected window. The measurements were repeated at each of the four windows to provide a velocity-travel curve for the whole cycle.

The measurements of fluid and particle velocity were obtained with the dual-beam, forward-scatter laser Doppler anemometer shown in Figure 2. Silicone oil droplets ($\approx 1\mu\text{m}$) were used to represent the gas flow and the anemometer was arranged, as in (3), with a 32 mW He-Ne laser, a focussing lens, a rotating diffraction grating, a collimating lens, a collecting lens and a photomultiplier. For the measurements of particle velocity, the anemometer was similar to that described above with a narrow slit in front of the collecting lens. The Doppler signals were processed by a purpose-built frequency counter with a sampling frequency of 22 KHz. The frequency counter was interfaced to a microcomputer which sampled the digital output of the counter and stored it in memory at a rate of about 10 KHz. The time information corresponding to each frequency count was obtained from a programmable timer module. The data was subsequently processed by the microcomputer to determine and display the variation of velocity as a function of time.

The initial pressure was 8 bars (gauge) and achieved with nitrogen taken from a pressurised cylinder. The initial pressure and the breech-pressure time record during the cycle were measured with a piezo-electric transducer and a charge amplifier whose output was digitised and interfaced to the microprocessor.

A detailed analysis of the errors associated with the experimental

techniques has been provided in (3). The maximum errors are 0.5%, 1%, 4% and 15% for pressure, projectile velocity and mean and rms values of fluid and particle velocity, respectively and are considered not to affect the conclusions.

3. Results and Discussion

3.1 Projectile dynamics

The measured projectile velocity-travel curves obtained with single-phase flow and with various initial chamber geometries are shown in Figure 3. The geometries include the gradual contraction of Figure 1, the gradual contraction with the particle-injector mechanism and the constant-diameter arrangement of (3). The velocity-travel curve obtained in the presence of particles is not included in this figure since it is identical to the single-phase curve. Figure 4 shows the corresponding breech-pressure time records and that the pressure variations of the constant diameter geometry are almost equal to the chambered geometry with the injector. The muzzle velocities are 45 m/s with the gradual contraction, 42 m/s with the particle injector installed and 40 m/s with the constant-diameter chamber; these differences stem mainly from the changes in loading parameter (mass of gas/mass of projectile) (6) associated with the differences in the initial volume of the three configurations. The initial volume with the gradual contraction, is 14% larger than that when the injector is fitted and there is 22% difference between the gradual contraction and the constant-diameter volumes. Calculations performed with the one-dimensional methods described in (3) using the isentropic variation of static pressure at the breech but taking into account the extra-volume due to chamberage, yielded results within 2% of the measurements; this confirms that the initial geometry has negligible effect on the projectile dynamics for the subsonic flows considered here.

3.2 Single-phase flow

In order to quantify the effect of gradual contraction on flow characteristics, and in particular on the growth of boundary layers, the mean and rms values of the axial velocity were obtained at the first window, computed for a time of 14.5 ms and plotted in profile form in Figure 5, where r denotes the radial position from the tube wall and R is the tube radius. The figure also shows the corresponding profiles obtained with the constant-diameter chamber of (3). With the gradual contraction, the mean velocities are higher by about 2 m/s (7%) due mainly to the difference in loading parameter and this is also evident in Figure 6 which shows the axial distributions of centreline mean velocity for the two chamber geometries and 26 ms after release of the projectile. The fluid velocities with the gradual contraction are higher at the axial locations corresponding to the first, second and third window, and the virtual origin established by extrapolating the measured values to a zero velocity is about $-0.92 x/d$ (-70 mm) which, corresponds to the extra volume associated with the gradual contraction.

The effect of initial chamber geometry on the mean flow characteristics in the wake of the projectile appears to be insignificant and the distributions of velocity in the initial volume and in the near upstream and downstream regions of the contraction are far from linear. The rms levels of the velocity fluctuations, are almost identical for the two geometries, with values of around 3% in the bulk of the flow and up to 9% in the boundary layer. The corresponding boundary layer thicknesses for the two geometries also compare well and were found to be 12% and 18% of the radius of the bore for 14.5 and 26 ms, respectively.

Fluid velocities were also measured with the gradual contraction and in the presence of the particle-injector mechanism and Figure 7 shows the profiles of mean and rms velocities obtained at the second window and at a time of 22 ms; the profiles obtained without the injector are also shown to allow comparisons. The profiles are almost

identical though within the boundary layer the injector case displays lower velocities, which is surprising since the loading parameters, and thus the projectile velocities, are different. The result can be explained for the core flow with reference to Figure 8 which shows the axial distributions of centreline mean velocity for the two cases and for a time of 26 ms. The origin of the axial distance in this figure, however, has been chosen to correspond to the virtual origin, (6), of the two configurations, rather than the geometric breech-position of Figure 6. It is clear that although the axial positions of the windows from the virtual origin (x') are different, the fluid velocities are within 5% of each other. This result also suggests that the injector mechanism does not affect the mean and turbulent nature of the flow fields in the barrel and in the wake of the projectile.

The nature of the boundary layers with the constant diameter chamber was addressed in (3) and they were found to be turbulent with characteristics similar to steady turbulent boundary layers. The boundary layers measured with the gradual contraction have, as expected, very similar features.

3.3 Two-phase flow

The velocities of the 500 μm particles were measured and can be compared with fluid velocities measured in the absence of the particles. The volume concentration of particles at the beginning of the cycle was around 1.3% and reduced to 0.3% at the end of the cycle, so that the particle-to-particle interaction can be assumed to be small throughout the cycle. The results are presented as ensemble mean and rms velocity profiles in Figure 9, together with the corresponding single-phase flow profiles. They were obtained in the first, second and third windows, corresponding to axial locations from the breech of 4.96d, 7.90d and 10.84d respectively, and are presented at different times in the cycle due to the variation in the occurrence and duration of the particle signal at different locations in the tube. Since the fluid velocities were measured in the absence of particles, conclusions about slip velocity need to be drawn with care. It can be seen that

the solid particles lag behind the fluid by times which increase with axial distance as the projectile is approached. The difference between the fluid and particle velocity increases in the bulk of the flow from about 1 m/s (3%) at $x/d = 4.96$ and $t = 20.5$ ms to 8 m/s (21%) at $x/d = 10.84$ and $t = 27.5$ ms. This lag is due to the inertial effects associated with solid particles in a strongly accelerating flowfield particularly in regions close to the projectile base. In this Lagrangian description therefore, the particles are always seen to lag behind the fluid phase, in the immediate vicinity of the projectile. The particle rms velocities are generally higher in the bulk of the flow than the corresponding single-phase values and the turbulence intensity at $x/d = 4.96$, for example, is almost 7% in the bulk flow in contrast to the single-phase value of about 4%. The higher rms levels observed with particles should be treated with caution, since the fluid rms values were measured in the absence of particles and the carrier phase should have a different turbulent field. Depending on the size, concentration and relaxation time of the particles, the turbulence structure can be modified by the particles and this may manifest itself as an increase in turbulence for particles with relatively large size and relaxation time (8 and 9). It is also probable that the increased levels can be associated with the initial boundary conditions imposed in the present experiments. Although the particle-injector mechanism was designed to minimise disturbance in the flow prevailing down the tube, and this was proven to be the case for the single-phase flow as previously discussed, it is possible that a disturbance superimposed on particle motion will survive throughout the cycle, contrary to its suppression for the carrier phase due to the stronger acceleration resulting from the expansion process and the gradual contraction introduced downstream of the injector. The particle rms levels are higher than the fluid phase in the bulk of the flow, they are very similar to those of the fluid near the wall and the effect of particles on wall boundary layer thickness seems to be weak.

The mean velocity profiles of figure 9 suggest that the particle boundary layers are of the same order of thickness as the fluid phase boundary layers which have been measured in the absence of particles.

The variation in the occurrence and duration of the particle signals at different locations in the barrel during the cycle, has made it impossible to obtain a complete profile within the boundary layer, but the measured turbulence intensities are consistent with those of the single-phase flow.

Figure 10 shows the centreline mean variation of particle and fluid velocity with time at $x/d = 4.96$, in a Eulerian frame. These mean values were evaluated from around 12 velocity traces two of which are also shown in Figure 10 for each phase. The fluid velocity is higher at the beginning of the cycle by about 2 m/s and by about 0.8 m/s at $t = 23$ ms. Later in the cycle as the projectile moves away the slip velocity changes sign, as the particles catch up and even lead the fluid phase. The flowfield at this fixed location decelerates with time, as seen on Figure 10, and the mean Reynolds number is also continuously decreasing with time. This situation is in agreement with the steady downflow of a solid/fluid suspension where it is known that, as the Reynolds number decreases, the lead of the particles over the fluid becomes progressively larger (7).

4. Conclusions

The main conclusions of this investigation follow:

- (1) The effect of initial chamber geometry on projectile motion as well as on flow characteristics in the wake of the projectile is found to be insignificant within the subsonic range considered and the relevant parameter is the ratio of the mass of gas/mass of projectile.
- (2) The comparison between the velocity of 500 μm Diakon particles and that of the fluid obtained separately in the absence of solid particles revealed that the particles lag behind the fluid in regions closer to the projectile because of their relatively large inertia and that the lag increases with axial distance from the breech reaching a measured maximum of about 20% near the end of the cycle.

(3) The observed rms levels of particle velocity are higher than those of the fluid in the bulk of the flow but attain similar values near the tube wall. This observation should, however, be treated with care since the fluid velocities were measured in the absence of the solid particles.

(4) At fixed locations in the barrel, the flowfield experiences deceleration and, for the same reason as in (2) above, the particle initially lags behind but later in the cycle leads the fluid slightly.

Acknowledgement

Financial support provided by the US Army research office is gratefully acknowledged. Technical assistance in the construction of the experimental rig, by Mr P Trowell is much appreciated.

References

1. Klingenberg G and Banks N E
"Review on interior and transitional ballistic research: state of the art of computational and experimental efforts".
EMI report Expl-Nr 028.
2. Gough P S.
"Modelling of two phase flows in guns".
Interior Ballistics of Guns, edited by H Kreer and M Summerfield, Vol 66, Progress in Astronautics and Aeronautics, 1979.
3. Bicen A P, Khezzar L and Whitelaw J E
"Subsonic single-phase flow in a gun simulator".
Mechanical Engineering Department Report, FS/86/03, Imperial College, London.
4. Bicen A P, Kliafas Y and Whitelaw J E.
"In-bore velocity measurements in the wake of a subsonic projectile".
AIAA J 24, 6, 1986.
5. Farrar C L and Leeming D W.
"Military Ballistics, a Basic Manual"
Brassey's Defence Publishers, 1983.
6. Seigel A E.
"The theory of high speed guns".
AGARDograph 91, 1965.
7. Mouri J, Yianneskis M and Whitelaw J E.
"Particle motion and turbulence in dense two-phase flows".
Mechanical Engineering Department Report, FS/86/24, Imperial College, London. To be published in J of Multiphase Flow.

8. Iraqi A.
"Turbulent particulate diffusion and dispersion between 2 parallel planes".
Doctorate Thesis, University of Rouen, France, 1965.

9. Owen P R.
"Pneumatic transport".
J Fluid Mech, 39, 2, 1969.

- Figure 1 Geometry of gun simulator and particle-injector mechanism.
- Figure 2 Schematic of experimental system.
- Figure 3 Projectile velocity-travel curves.
- Figure 4 Breech-pressure time records.
- Figure 5 Effect of initial chamber geometry on single-phase flow characteristics.
- Figure 6 Axial distributions of centreline mean velocity for initial chambers with constant-diameter and gradual contraction; $t = 26 \text{ ms}$.
- Figure 7 Effect of particle-injector mechanism on single-phase flow characteristics.
- Figure 8 Axial distributions of centreline mean velocity with and without particle-injector mechanism.
- Figure 9 Radial profiles of mean and rms axial velocities of particles and fluid.
- Figure 10 Centreline mean velocities of particles and fluid during ballistic cycle and at $x = 4.96d$.

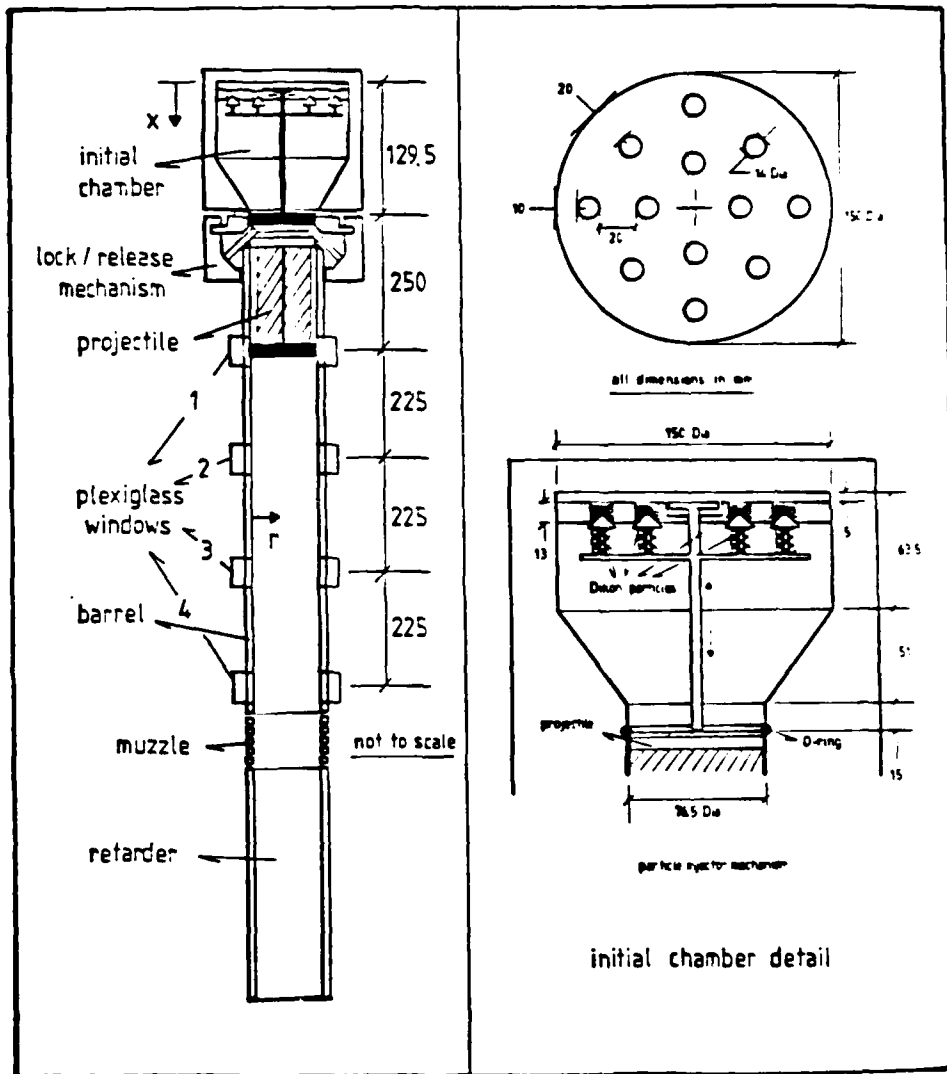


Figure 1 Geometry of gun simulator and particle-injector mechanism.

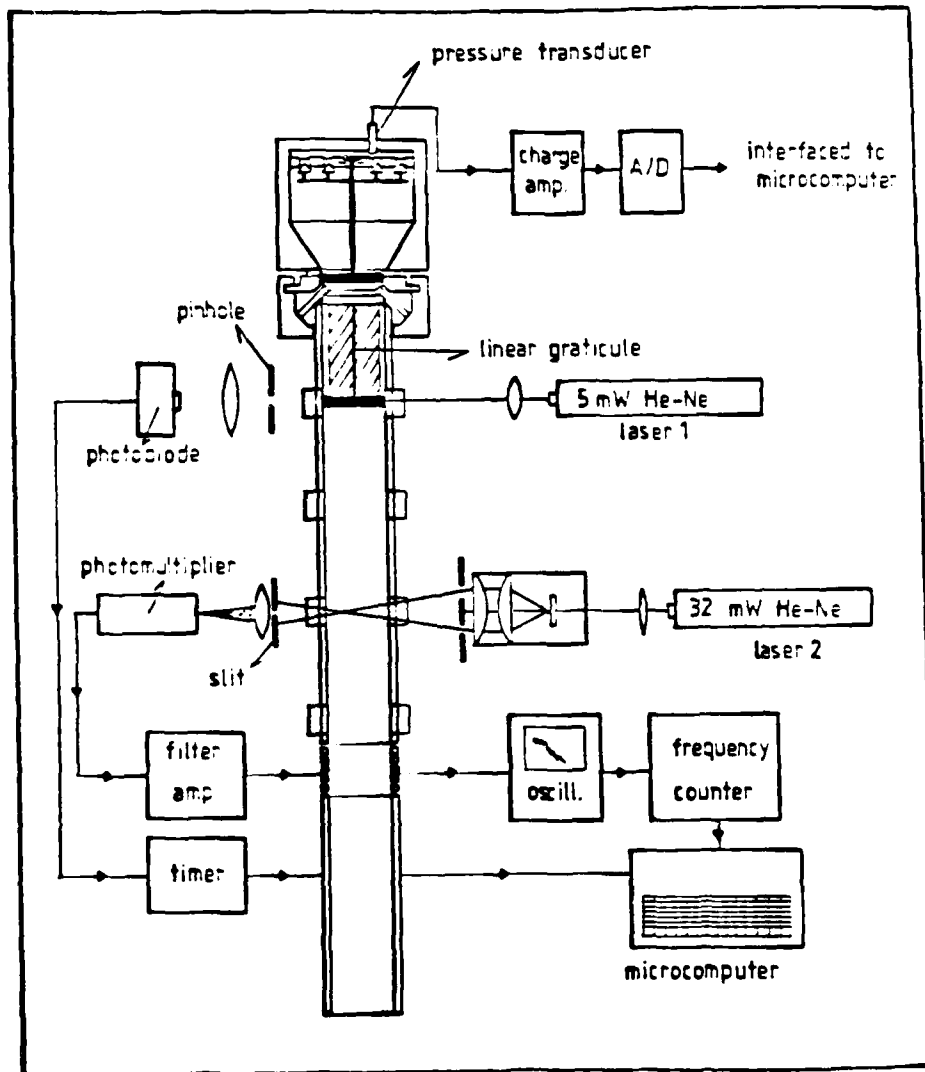


Figure 2 Schematic of experimental system.

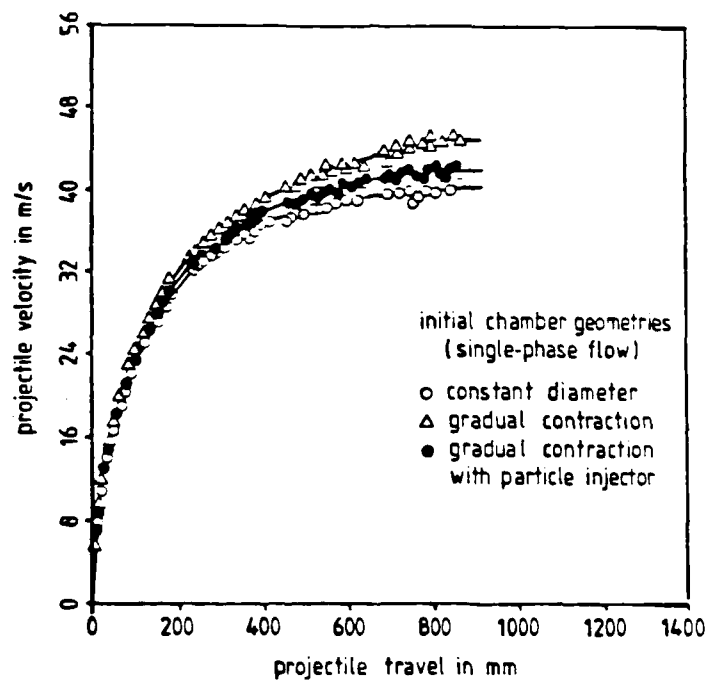


Figure 3 Projectile velocity-travel curves.

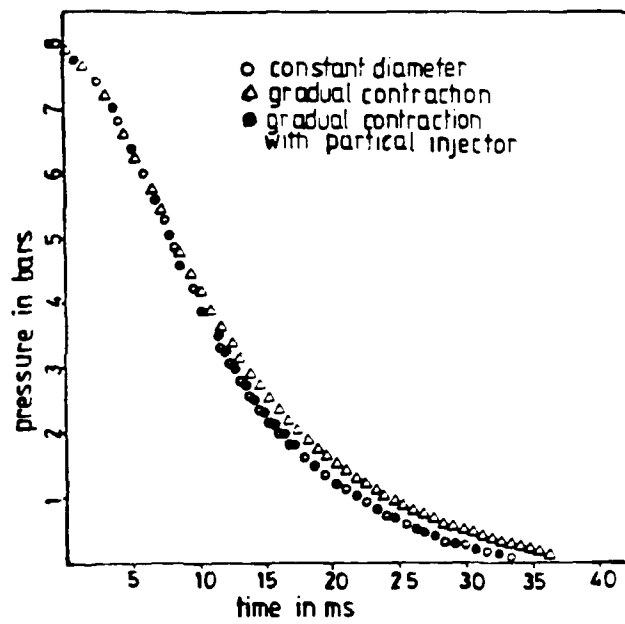


Figure 4 Breech-pressure time records.

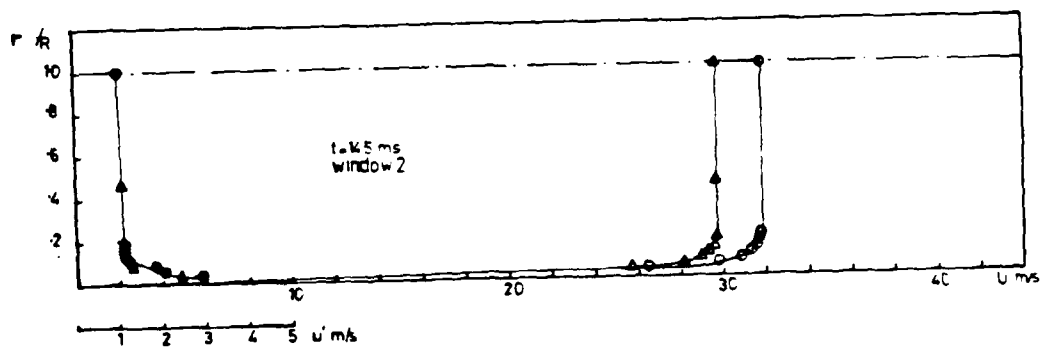


Figure 5 Effect of initial chamber geometry on single-phase flow characteristics.

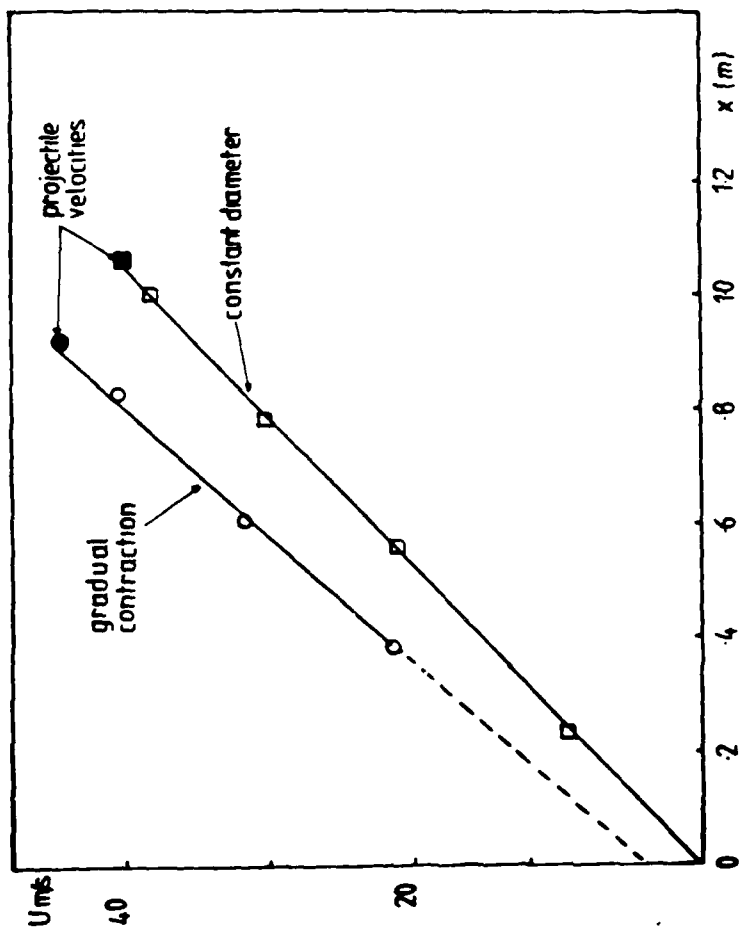


Figure 6 Axial distributions of centreline mean velocity for initial chambers with constant-diameter and gradual contraction; $t = 26$ ms.

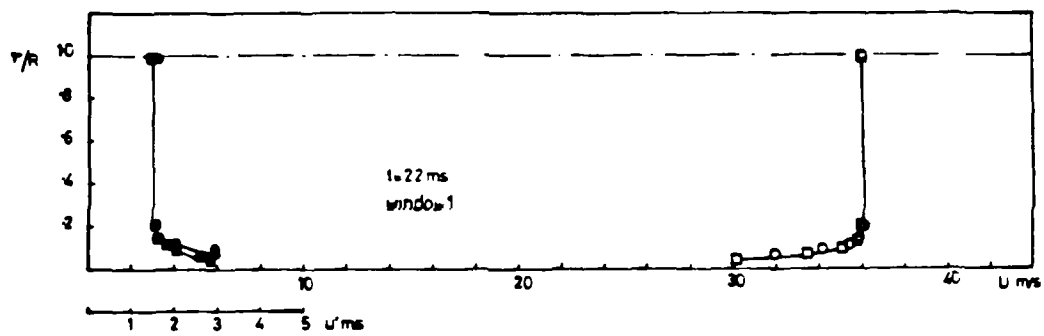


Figure 7 Effect of particle-injector mechanism on single-phase flow characteristics.

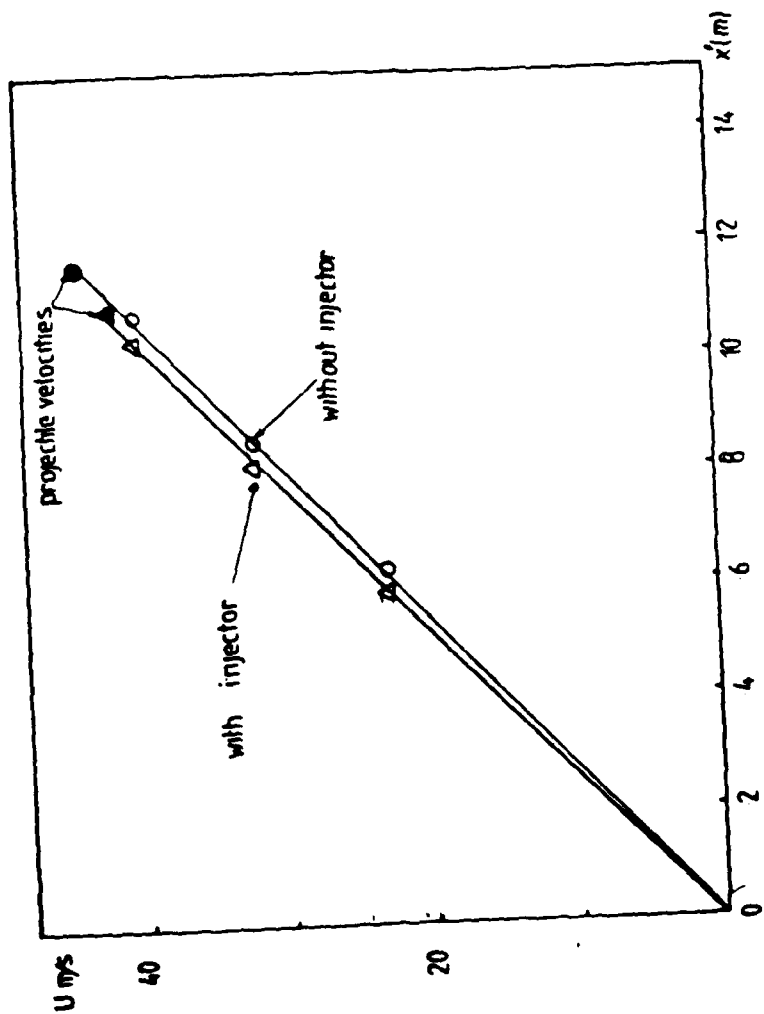


Figure 8 Axial distributions of centerline mean velocity with and without particle-injector mechanism.

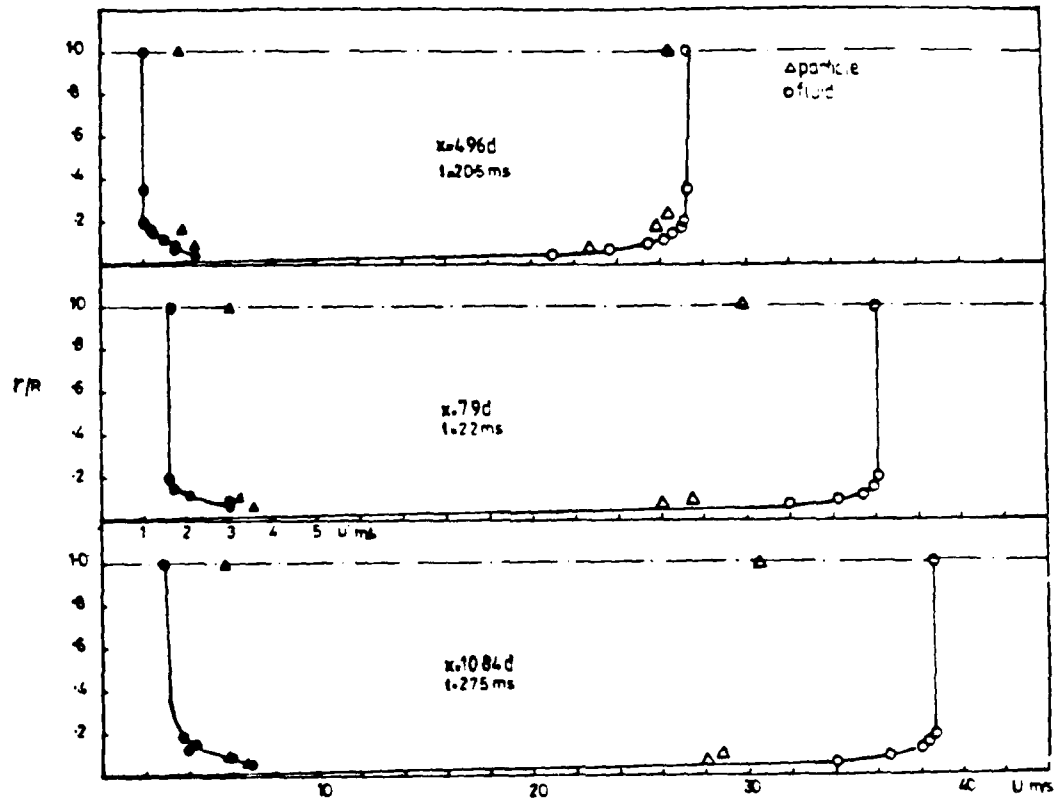


Figure 9 Radial profiles of mean and rms axial velocities of particles and fluid.

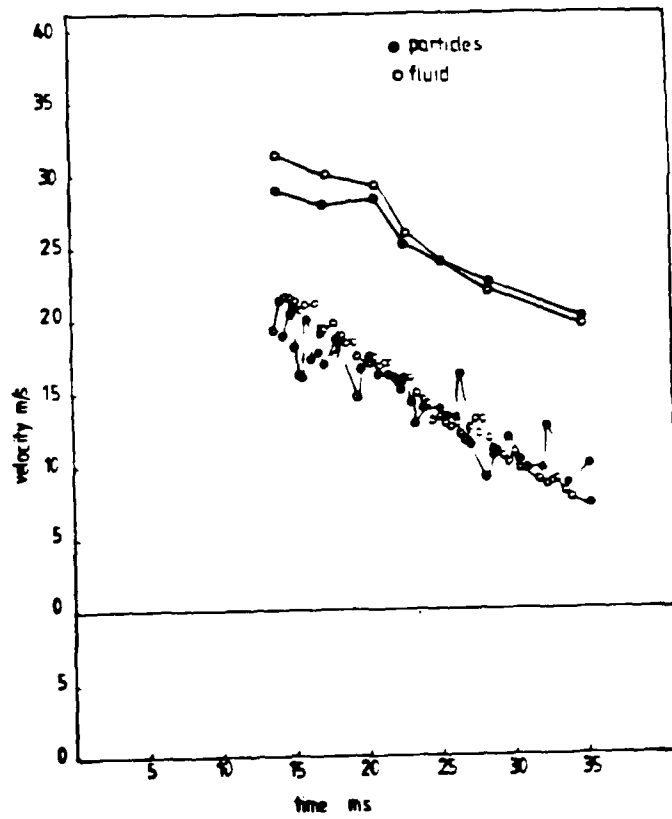


Figure 10 Centrelines mean velocities of particles and fluid during ballistic cycle and at $x = 4.96d$.

END

DATE
FILMED

3 88

ITL